

A theory of jet shapes and cross sections: from hadrons to nuclei

Ivan Vitev,¹ Simon Wicks,² and Ben-Wei Zhang^{1,3}

¹*Los Alamos National Laboratory, Theoretical Division, MS B238, Los Alamos, NM 87545, USA*
²*Department of Physics, Columbia University, 538 West 120-th Street, New York, NY 10027, USA*
³*Institute of Particle Physics, Hua-Zhong Normal University, Wuhan, 430079, China*

(Dated: October 30, 2018)

For jets, with great power comes great opportunity. The unprecedented center of mass energies available at the LHC open new windows on the QGP: we demonstrate that jet shape and jet cross section measurements become feasible as a new, differential and accurate test of the underlying QCD theory. We present a first step in understanding these shapes and cross sections in heavy ion reactions. Our approach allows for detailed simulations of the experimental acceptance/cuts that help isolate jets in such high-multiplicity environment. It is demonstrated for the first time that the pattern of stimulated gluon emission can be correlated with a variable quenching of the jet rates and provide an approximately model-independent approach to determining the characteristics of the medium-induced bremsstrahlung spectrum. Surprisingly, in realistic simulations of parton propagation through the QGP we find a minimal increase in the mean jet radius even for large jet attenuation. Jet broadening is manifest in the tails of the energy distribution away from the jet axis and its quantification requires high statistics measurements that will be possible at the LHC.

PACS numbers:

I. INTRODUCTION

Fast partons propagating in a hot/dense nuclear medium are expected to lose a large fraction of their energy [1]. In fact, the stopping power of strongly-interacting matter for color-charged particles has, by far, the largest experimentally established effect: the attenuation of the cross section for final-state observables of large mass/momentum/energy. This jet quenching mechanism has been used to successfully explain the strong suppression of the hadron spectra at large transverse momentum observed in nucleus-nucleus collisions at the Relativistic Heavy Ion Collider (RHIC) [2, 3]. There is mounting evidence that the quark-gluon plasma (QGP)-induced quenching can be disentangled from other nuclear effects even at the much lower Super Proton Synchrotron (SPS) center of mass energy [4]. To calculate parton energy loss in the QGP several theoretical approaches have been developed [5, 6, 7, 8]. While tackling the same basic problem, they use different assumptions for the boundary conditions (initial/final quark or gluon virtuality), make different approximations for the parent parton and radiative gluon kinematics, and treat differently the interaction between the jet+gluon system with the medium (differentially vs on average). For discussion see [9].

At present, most measurements of hard processes are limited to single particles and particle correlations, which are only the leading fragments of a jet. There is general agreement on the physics that controls inclusive particle suppression in the QGP and the experimental methodology of determining $R_{AA}(p_T)$ (or $I_{AA}(p_{T_1}, p_{T_2})$) [2]. Thus, for any particular combination of radiative/collisional energy loss evaluation and its phenomenological application to leading particle quenching the QGP density can be determined with 20 – 25% “statistical” accuracy [10]. An

inherent limitation of this approach is that while fits to the data can, not surprisingly, always be performed [11] they do not resolve the staggering order of magnitude “systematic” discrepancy in the extracted medium properties. Furthermore, focusing on quantities that can be constrained with little ambiguity from the measured rapidity entropy density in heavy ion collisions distracts from issues such as the approximations that go into theoretical energy loss derivations and their application to systems where more often than not these initial assumptions are violated [42]. In searching for experimental measurements which can pinpoint the framework for energy loss calculations that is applicable to heavy ion reactions, complex multi-particle correlations may not be optimal. They are very sensitive to non-perturbative effects/fragmentation and the modeling effort cannot be systematically improved due to the violation of factorization for highly exclusive observables [12]. It is, therefore, critical to find alternatives that accurately reflect the energy flow in strongly-interacting systems and have a more direct connection to the underlying quantum chromodynamics (QCD) theory.

The intra-jet energy distribution and the related cross section for jets in the case of heavy ion reaction closely match the criteria outlined above. The high rate of hard probes at the LHC and the large-acceptance calorimetry, see e.g. [13], will enable these accurate measurements. It should be noted that proof-of-principle measurements of jet cross sections have become possible at RHIC [14], but significantly better statistics will be required to quantify the QGP effects on jets. In this paper we study the magnitude of these modifications in Pb+Pb collisions at $\sqrt{s} = 5.5$ TeV at LHC. We demonstrate that a natural

generalization of leading particle suppression to jets,

$$R_{AA}^{\text{jet}}(E_T; R^{\text{max}}, \omega^{\text{min}}) = \frac{\frac{d\sigma^{AA}(E_T; R^{\text{max}}, \omega^{\text{min}})}{dy d^2 E_T}}{\langle N_{\text{bin}} \rangle \frac{d\sigma^{pp}(E_T; R^{\text{max}}, \omega^{\text{min}})}{dy d^2 E_T}}, \quad (1)$$

is sensitive to the nature of the medium-induced energy loss. The steepness of the final-state differential spectra amplifies the observable effect and the jet radius R^{max} and the minimum particle/tower energy $p_{T \text{ min}} \approx \omega^{\text{min}}$ provide, through the evolution of $R_{AA}^{\text{jet}}(E_T; R^{\text{max}}, \omega^{\text{min}})$ at any fixed centrality, experimental access to the QGP response to quark and gluon propagation.

In the following discussion of jet shapes and jet cross sections in p+p and A+A collisions we stay as close as possible to an analytic theoretical approach. Thus, we are able to unambiguously connect the non-perturbative QCD effects, medium properties and the induced bremsstrahlung spectrum to experimental jet observables. Determination of baseline jet shapes and their generalization to finite momentum acceptance cuts builds upon the work of Seymour [15]. We refer the reader to [15, 16] for discussion of the complications in defining a jet and the related topic of jet-finding algorithms. To make the discussion simpler, we will assume that the complications of the different definitions can be subsumed into an R_{sep} parameter, as described in Appendix B. Once a jet axis and all of the jet particles / calorimeter towers “i” have been identified, the “integral jet shape” is defined as:

$$\Psi_{\text{int}}(r; R) = \frac{\sum_i (E_T)_i \Theta(r - (R_{\text{jet}})_i)}{\sum_i (E_T)_i \Theta(R - (R_{\text{jet}})_i)} \quad (2)$$

where r, R are Lorentz-invariant opening angles, $R_{ij} = \sqrt{(\eta_i - \eta_j)^2 + (\phi_i - \phi_j)^2}$, and i represents a sum over all the particles in this jet. $\Psi_{\text{int}}(r; R)$ is the fraction of the total energy of a jet of radius R within a subcone of radius r . It is automatically normalized so that $\Psi_{\text{int}}(R; R) = 1$. To move from the integrated to the differential jet shape, we define:

$$\psi(r; R) = \frac{d\Psi_{\text{int}}(r; R)}{dr}. \quad (3)$$

This is the angular density of jet energy (remembering that the appropriate 3D representation would be $\psi^{\text{vis}}(r; R) = \frac{1}{2\pi r} \psi(r; R)$). Understanding the many-body QCD theory behind jet shape calculations will naturally lead to understanding the attenuation of jets in reactions with heavy nuclei.

This article is organized as follows: in Section II, we outline a calculation of the jet shape in nucleon-nucleon (N+N) collisions using the framework of perturbative QCD. We compare this calculation to existing Tevatron data and investigate the jet shapes at LHC energies. A brief discussion of final-state QGP-induced radiative energy loss in the GLV formalism is given in Section III. We prove that the cancellation of small-angle near-jet

axis bremsstrahlung persists to all orders in the correlation between the multiple scattering centers and provide details of its numerical evaluation. The fully differential distribution of the energy lost by a hard parton is also shown. In Section IV we present results for the medium-modified jet shapes and cross sections as a function of the jet cone radius, R , and the experimental p_T cut, ω_{min} , and discuss a simple energy sum rule. We demonstrate the connection between the characteristic properties of the QGP-induced gluon radiation and the variable suppression, at the same impact parameter b , of jet rates, the modulation of the mean jet radius and the enhancement in the “tails” of the intra-jet energy flow distribution. A summary and conclusions are presented in Section V. Appendix A shows a calculation of the baseline jet cross sections at the LHC and an estimate of the accuracy with which these cross sections and jet shapes can be measured with nominal first-year integrated luminosities in p+p and A+A reactions. In Appendix B we study the influence of the different perturbative and non-perturbative contributions to the jet shape in hadronic collisions. Finally, Appendix C contains a discussion of a double differential measure of energy flow in jets and its connection to particle angular correlation measurements, currently conducted at RHIC.

II. JET SHAPES IN ‘ELEMENTARY’ P-P COLLISIONS

In the process of advancing perturbative QCD theory to many-nucleon systems, the final-state experimental observables should be first understood in the simpler p+p reactions.

A. Theoretical considerations

1. Leading order results

In the introduction, we defined the central quantity of our study, the differential jet shape for parton “a”, $\psi_a(r; R)$. As in [15], the starting point of the calculation is the leading order parton splitting: a suitable separation of physical time scales enables the separation of the calculation into production and jet showering. The QCD splitting functions $P_{a \rightarrow bc}(z)$ give the distribution of the large fractional lightcone momenta (or approximately the energy fractions) of the fragments relative to the parent parton, z and $1 - z$ respectively. To lowest order, recalling that $\psi_a(r; R)$ describes the energy flow $\propto z$, we can write:

$$\psi_a(r; R) = \frac{d\Psi_{\text{int},a}(r; R)}{dr} = \sum_b \frac{\alpha_s}{2\pi} \frac{2}{r} \int_{z_{\text{min}}}^{1-Z} dz z P_{a \rightarrow bc}(z). \quad (4)$$

In Eq. (4) $r = (1 - z)\rho$ is related to the opening angle ρ between the final-state partons.

In ‘‘elementary’’ p+p collisions the inclusion of soft particles ($z_{min} \approx 0$) in theoretical calculations is not a bad approximation. Even in this case, however, there are intrinsic limitations on the minimum particle/calorimeter tower p_T or E_T , related, for example, to detector acceptance. In heavy ion reactions, especially for the most interesting case of central collisions, there is an enormous background of soft particles related to the bulk QGP properties. Jet studies will likely require minimum particle energy $> 1 - 2$ GeV at RHIC and even more stringent cuts at the LHC. Furthermore, control over z_{min} can provide detailed information about the properties of QGP-induced bremsstrahlung. Further kinematic constraints on the values of z arise since both the resulting partons must be within an angular distance R of the original jet axis, $r < R$, $rz/(1-z) < R$. In this case they are identified with the jet. If not, they are identified as two separate jets. For a cone-based algorithm, the relative separation $R_{sep}R$ (as opposed to just the distance from the original jet axis) is an additional criterion: $\rho < R_{sep}R$. We find:

$$Z = \max \left\{ z_{min}, \frac{r}{r+R} \right\} \text{ if } r < (R_{sep} - 1)R, \quad (5)$$

$$Z = \max \left\{ z_{min}, \frac{r}{R_{sep}R} \right\} \text{ if } r > (R_{sep} - 1)R. \quad (6)$$

Carrying out the integration in Eq. (4) we arrive at the LO jet shape functions for quarks and gluons:

$$\psi_q(r) = \frac{C_F \alpha_s}{2\pi} \frac{2}{r} \left(2 \log \frac{1-z_{min}}{Z} - \frac{3}{2} [(1-Z)^2 - z_{min}^2] \right), \quad (7)$$

$$\begin{aligned} \psi_g(r) = & \frac{C_A \alpha_s}{2\pi} \frac{2}{r} \left(2 \log \frac{1-z_{min}}{Z} - \left(\frac{11}{6} - \frac{Z}{3} + \frac{Z^2}{2} \right) (1-Z)^2 \right. \\ & \left. + \left(2z_{min}^2 - \frac{2}{3}z_{min}^3 + \frac{1}{2}z_{min}^4 \right) \right) \\ & + \frac{T_R N_f \alpha_s}{2\pi} \frac{2}{r} \left(\left(\frac{2}{3} - \frac{2Z}{3} + Z^2 \right) (1-Z)^2 - \left(z_{min}^2 - \frac{4}{3}z_{min}^3 + z_{min}^4 \right) \right). \quad (8) \end{aligned}$$

In the $z_{min} \rightarrow 0$ limit Eqs. (7) and (8) reduce and we recover the previously known results [15]. There is an implicit ‘plus-prescription’ in these results when calculating moments of physical quantities, as we have not considered the virtual corrections in the forward direction. Hence, the result is not applicable for $r = 0$ and does not have the correct normalization when integrated. However, the shape is reflective of final-state parton splitting and, when needed, for the leading order calculation one may apply a cutoff for small r and normalize via first-bin subtraction.

In contrast to the case of $e^+ + e^-$ annihilation, hadronic scattering is accompanied by copious initial-state radiation (ISR) that can fall within the jet cone. While the contribution of the ISR is small for small values of r/R , it gives an essential contribution at larger angles. A simple estimate based on a dipole radiation and the kinematics of the hard parton - soft gluon coincidence within a cone [15], similar for both quark and gluon jets, yields:

$$\psi_i(r) = \frac{C\alpha_s}{2\pi} 2r \left(\frac{1}{Z^2} - \frac{1}{(1-z_{min})^2} \right), \quad (9)$$

Again, the ‘plus-prescription’ to account for the $r = 0$ point is not explicitly shown. In Eq. (9) $C \simeq C_F \approx C_A/2$.

The leading order calculation is most appropriate for the rare, hard splittings of a very high momentum jet. The use of a running coupling improves the numerical results, providing larger weight for softer events. We employ a running α_s evaluated at the largest k_T in the problem, $\mu = r(1-Z)E_T$ for the jet splitting and $\mu = (1-Z)E_T$ for the initial state radiation [15].

2. Resummation - all orders and multiple emission

As $r \rightarrow 0$, in the collinear limit of parton splitting, the leading order contributions to the jet shape diverge, see Eqs. (7), (8) and (9). In fact, all orders in the perturbative expansion diverge, including powers of $\log r$ in the form $\alpha_s^n \log^{2n-1} r$. With plentiful parton showering, it becomes increasingly less likely that any particular quark and gluon will be coincident with the jet axis. Quantitatively, this is described by a Sudakov form factor. The energy density at small angles is dominated by the hard parton in the splitting. If there is a splitting that leaves the hard parton at an angle r_1 , a subsequent splitting at $r_2 < r_1$ will not contribute to the energy density at r_2 . Multiple independent splitting follows a Poisson distribution, hence, the probability of energy flow at an angle less than r is exponentially suppressed by the integrated probability at angles greater than r , i.e.:

$$P(< r) = \exp(-P_1(> r)) \quad (10)$$

$$= \exp \left(- \int_r^R dr' \psi_{coll}(r') \right). \quad (11)$$

This only applies for soft emissions which do not take away (much) momentum, i.e. at leading log accuracy. Improvement can be obtained at modified leading log accuracy (MLLA), when the running of the coupling constant is included in P_1 . We don’t take other (e.g. recoil or kinematic constraints) effects in evaluating the Sudakov form factor in the soft collinear approximation.

The resummed $\psi_{resum}(r) = \frac{d}{dr} P(< r)$ and we carry out the integration in Eq. (11), including the running $\alpha_s(rE_T)$, to obtain modified leading logarithmic accuracy (MLLA). Note that $\alpha_s(\mu) = 1/(2\beta_0 \log \frac{\mu}{\Lambda_{QCD}})$, with $4\pi\beta_0 = b_0 = \frac{11}{3}C_A - \frac{4}{3}T_R N_f$. First, take the small r

limit in Eqs. (7), (8) and (9), keeping terms $\propto 1/r$ and $\propto 1/r \log(1/r)$. Based on $Z = \max(z_{min}, r/R)$, in this limit we have two kinematic domains. For $r > z_{min}R$ the results are similar to the known case of no acceptance cut-off and reduce to the known results if $z_{min} = 0$:

$$P_q(r > z_{min}R) = \exp\left(2C_F \log \frac{R}{r} f_1\left(2\beta_0 \alpha_s \log \frac{R}{r}\right) - \left[\frac{3}{2}C_F - CR^2 - c_q^>(z_{min})\right] \times f_2\left(2\beta_0 \alpha_s \log \frac{R}{r}\right)\right), \quad (12)$$

$$P_g(r > z_{min}R) = \exp\left(2C_A \log \frac{R}{r} f_1\left(2\beta_0 \alpha_s \log \frac{R}{r}\right) - \left[\frac{1}{2}b_0 - CR^2 - c_g^>(z_{min})\right] \times f_2\left(2\beta_0 \alpha_s \log \frac{R}{r}\right)\right). \quad (13)$$

It is useful to employ the same notation as in [15] and facilitate the comparison to the case of no kinematic cuts: $f_1(x) = \log(1-x)/(2\pi\beta_0)$, and $f_2(x) = (1 - \log(1-x)/x)/(2\pi\beta_0)$. The z_{min} -dependent corrections are isolated as follows:

$$c_q^>(r > z_{min}R; z_{min}) = 2C_F \log(1 - z_{min}) + \frac{3}{2}C_F z_{min}^2, \quad (14)$$

$$c_g^>(r > z_{min}R; z_{min}) = 2C_A \log(1 - z_{min}) + C_A \left(2z_{min}^2 - \frac{2}{3}z_{min}^3 + \frac{1}{2}z_{min}^4\right) - T_R N_f \left(z_{min}^2 - \frac{4}{3}z_{min}^3 + z_{min}^4\right). \quad (15)$$

When $r < z_{min}R$ the integration in Eq. (11) has to be split in two regions: $r' \in (r, z_{min}R)$ and $r' \in (z_{min}R, R)$. The second integral is trivially obtained from the case that was just considered above, Eqs. (12) and (13), with the substitution $r = z_{min}R$. When combined with the first integral, it yields:

$$P_q(r < z_{min}R) = P_q(r > z_{min}R; r = z_{min}R) \times \exp\left(-\left[\frac{3}{2}C_F - c_q^<(z_{min})\right] \times f_2\left(2\beta_0 \tilde{\alpha}_s \log \frac{z_{min}R}{r}\right)\right), \quad (16)$$

$$P_g(r < z_{min}R) = P_g(r > z_{min}R; r = z_{min}R) \times \exp\left(-\left[\frac{1}{2}b_0 - c_g^>(z_{min})\right] \times f_2\left(2\beta_0 \tilde{\alpha}_s \log \frac{z_{min}R}{r}\right)\right). \quad (17)$$

Here, we denote by $\tilde{\alpha}_s = \alpha_s(z_{min}RE_T)$, as opposed to

$\alpha_s = \alpha_s(RE_T)$, and:

$$c_q^<(r < z_{min}R; z_{min}) = 2C_F \log\left(\frac{1 - z_{min}}{z_{min}}\right) + 3C_F z_{min}, \quad (18)$$

$$c_g^<(r < z_{min}R; z_{min}) = 2C_A \log\left(\frac{1 - z_{min}}{z_{min}}\right) + C_A \left(4z_{min} - z_{min}^2 + \frac{2}{3}z_{min}^3\right) - T_R N_f \left(2z_{min} - 2z_{min}^2 + \frac{4}{3}z_{min}^3\right). \quad (19)$$

Note that the Sudakov form factors evaluated here will regulate any collinear divergence present in ψ_{coll} .

3. Power corrections - an estimate of non-perturbative effects

Inclusion of the running coupling constant under the momentum transfer integrals yields contributions from regions in which $Q \sim \Lambda_{QCD}$ or lower, i.e. there is a fundamental non-perturbative contribution to all of the integrals. An estimate of these power correction effects with finite acceptance gives the following result:

$$\psi_{PC}(r) = \frac{2C_R}{2\pi} \frac{2}{r} \frac{Q_0}{rE_T} \left(\bar{\alpha}_0'(Q_0, k_{min}) - \alpha_s(\mu) - 2\beta_0 \alpha_s(\mu)^2 \left(1 + \log \frac{\mu}{Q_0}\right) + \frac{2C_R}{2\pi} \frac{2}{r} \frac{k_{min}}{rE_T} \left(\alpha_s(\mu) + 2\beta_0 \alpha_s(\mu)^2 \left(1 + \log \frac{\mu}{k_{min}}\right) \right) \right), \quad (20)$$

where $C_R = C_F, C_A$ for quarks or gluons, respectively. In Eq. (20) $k_{min} = z_{min}rE_T$ and μ is the renormalization scale. The term $\propto \bar{\alpha}_0'(Q_0, k_{min})$ depends on the parametrized non-perturbative contribution, defined as:

$$\bar{\alpha}_0'(Q_0, k_{min}) = \frac{1}{Q_0} \int_{k_{min}}^{Q_0} dk \alpha_s(k), \quad (21)$$

with Q_0 representing the non-perturbative scale. In our numerical calculation we use

$$\bar{\alpha}_0'(2 \text{ GeV}, 0) = 0.52, \quad \bar{\alpha}_0'(3 \text{ GeV}, 0) = 0.42 \quad (22)$$

from Ref. [15, 18] and a parametrization of the strong coupling constant at small momentum transfer given in Ref. [19]. The terms $\propto \alpha_s(\mu), \alpha_s^2(\mu)$, come from subtracting the perturbative component in the non-perturbative region [18]. Finally, the term $\propto k_{min}$ results from the introduction of finite acceptance, z_{min} .

A similar expression is derived for initial-state radiation:

$$\begin{aligned} \psi_{i,PC}(r) = & \frac{2C}{2\pi} 2r \frac{Q_0}{E_T} \left(\bar{\alpha}_0'(Q_0, k'_{min}) - \alpha_s(\mu) \right. \\ & \left. - 2\beta_0 \alpha_s(\mu)^2 \left(1 + \log \frac{\mu}{Q_0} \right) \right) \\ & + \frac{2C_R}{2\pi} 2r \frac{k'_{min}}{E_T} \left(\alpha_s(\mu) \right. \\ & \left. + 2\beta_0 \alpha_s(\mu)^2 \left(1 + \log \frac{\mu}{k'_{min}} \right) \right), \quad (23) \end{aligned}$$

where $k'_{min} = z_{min} E_T$, and $C \simeq C_F \approx C_A/2$. At lower jet energies the power corrections are, in fact, sizable even at large r . This suggests that if there is deviation between the theoretical results and the experimental data it may be largely due to incomplete consideration of non-perturbative effects. We stress that the generalization of power corrections to finite acceptance implies that these should be taken into account only for $z_{min} r E_T < Q_0$ or $z_{min} E_T < Q_0$ for final-state and initial-state radiation, respectively.

4. Total contribution to the jet shape

As indicated before, the resummed jet shape at small r/R is evaluated as $\psi_{resum}(r) = \frac{d}{dr} P(r) = \psi_{coll}(r) P(r)$. Taking all contributions to the jet shape and ensuring that there is no double counting at small r/R to $\mathcal{O}(\alpha_s)$ we find:

$$\begin{aligned} \psi(r) = & \psi_{coll}(r) (P(r) - 1) + \psi_{LO}(r) + \psi_{i,LO}(r) \\ & + \psi_{PC}(r) + \psi_{i,PC}(r), \quad (24) \end{aligned}$$

On the right-hand-side of Eq. (24) the first term comes from Sudakov resummation with subtraction of the leading $1/r$, $(1/r) \log(1/r)$ contribution at small r/R to avoid double counting with the fixed order component of the differential jet shape. The second and third terms represent the leading-order contributions in the final-state and the initial-state. The last two terms represent the effect of power corrections. In a full calculation the relative quark and gluon fractions $f_q + f_g = 1$ are also needed: $\psi(r; E_T) = f_q(E_T, \sqrt{s}) \psi_q(r; E_T) + f_g(E_T, \sqrt{s}) \psi_g(r; E_T)$. These fractions are calculated in Appendix A alongside the demonstration of the feasibility of jet cross section and differential jet shape measurements at $\sqrt{s} = 5.5$ TeV.

If the resummed part completely dominates the area under $\psi(r)$ in Eq. (24), i.e. the power corrections and the fixed order result affect only the large r/R “tails”, the theoretically calculated differential jet shape is properly normalized. In reality, this is not the case and the first correction, $\mathcal{O}(\alpha_s^2)$, arises from $\psi_{coll}(r)(P(< r) - 1) = \psi_{coll}(r)(1 + C_R \alpha_s(\dots) + \dots - 1)$. It will be larger for gluon jets when compared to quark jets, C_A vs C_F , and for

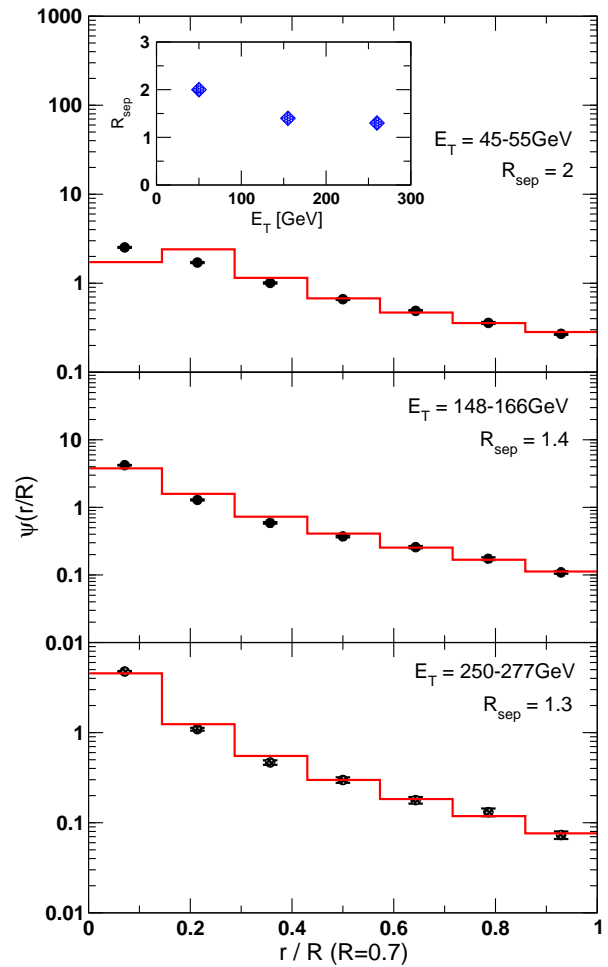


FIG. 1: (Color online) Comparison of numerical results from our theoretical calculation to experimental data on differential jet shapes at $\sqrt{s} = 1960$ GeV by CDF II [20]. Insert shows the E_T dependence of R_{sep} .

lower transverse energies. The normalization can then be ensured via

$$\psi(r) \rightarrow \psi(r) + \text{Norm} \times \psi_{coll}(r) \ln(P(< r)), \quad (25)$$

where Norm is determined numerically. We stress that to achieve a robust theoretical description of the differential jet shape all contributions to $\psi(r)$ from Eq. (24) should be included. In Appendix B we elucidate their relative strength using numerical examples. We also investigate the dependence of the shape on R_{sep} and the non-perturbative scale Q_0 .

B. Comparison to the Tevatron data

In Fig. 1 we show comparison of the theoretical model for the jet shape, Eq. (24), to the experimental measurements in $p + \bar{p}$ collisions at $\sqrt{s} = 1960$ GeV at Fermilab from Run II (CDF II) [20]. Our numerical results include all contributions from leading order, resummation and

power corrections with $Q_0 = 2$ GeV. The insert shows the variation of the parameter R_{sep} with the transverse energy of the jet. At high jet E_T our theoretical model gives very good descriptions of the large r/R experimental data with $R_{sep} = 1.3 - 1.4$. For $E_T = 45 - 55$ GeV the largest meaningful value $R_{sep} = 2$ can describe the data fairly well, except at very small r/R region. Extended discussion of the various contributions to the differential jet shape is given in Appendix B.

We note that for $r/R \ll 1$ and a large gluon jet fraction in conjunction with moderate $E_T \leq 50$ GeV there is still deviation between the data and the theory, e.g. the top panel of Fig. 1. This is likely related to the need for significant corrections, Eq. (25), to ensure the proper normalization of $\psi(r/R)$. Such corrections, in turn, point to NLO effects, a possible breakdown of our soft collinear jet splitting approximation for the Sudakov resummation and non-perturbative effects. Note that even Monte Carlo event generators have to be tuned to describe this data [20]. For the purpose of our manuscript the deficiencies in this specific part of phase space are not essential since, as we will see in Section IV, the experimental signatures of jet propagation in the QGP are most pronounced in the complementary $r/R \sim 1$ domain. One simply has to keep in mind that the description of $r/R < 0.25$ $\psi(r/R)$ in the vacuum allows for further theoretical improvement.

C. Predictions for the LHC

We employ the theoretical model that describes the CDF II data and apply the same transverse energy-dependent R_{sep} parameter to obtain predictions for the LHC at $\sqrt{s} = 5.5$ TeV. The emphasis here is to produce a baseline in $p + p$ reactions for comparison to the full in-medium jet shape in $Pb + Pb$ collisions. The essential difference in going from the Tevatron to the LHC is in the production of hard jets. At the higher collision energy we observe a greater contribution from gluon jets relative to quark jets, e.g. Fig. 12 in Appendix A. Therefore, for the same E_T , jets at the LHC are expected to be slightly wider than at the Tevatron.

Figure 2 shows our numerical results for the jet shape for four different energies $E_T = 50, 100, 250, 500$ GeV and two cone radii $R = 0.7, 0.4$ in $p + p$ collisions at $\sqrt{s} = 5.5$ TeV at LHC. An interesting observation is that, when plotted against the relative opening angle r/R , these shapes are self-similar, i.e. approximately independent of the absolute cone radius R . One of the main theoretical developments in this paper is the analytic approach to studying finite detector acceptance effects or experimentally imposed low momentum cuts. In Fig. 2 this is illustrated via the selection of $z_{min} = p_{T\ min}/E_T = 0.2, 0.1, 0.04$ and 0.02 ($p_{T\ min} = \omega^{\min} = 10$ GeV). Eliminating the soft partons naturally leads to a narrower branching pattern. However, for this effect to be readily observable 10 – 20% of the jet energy, going into soft

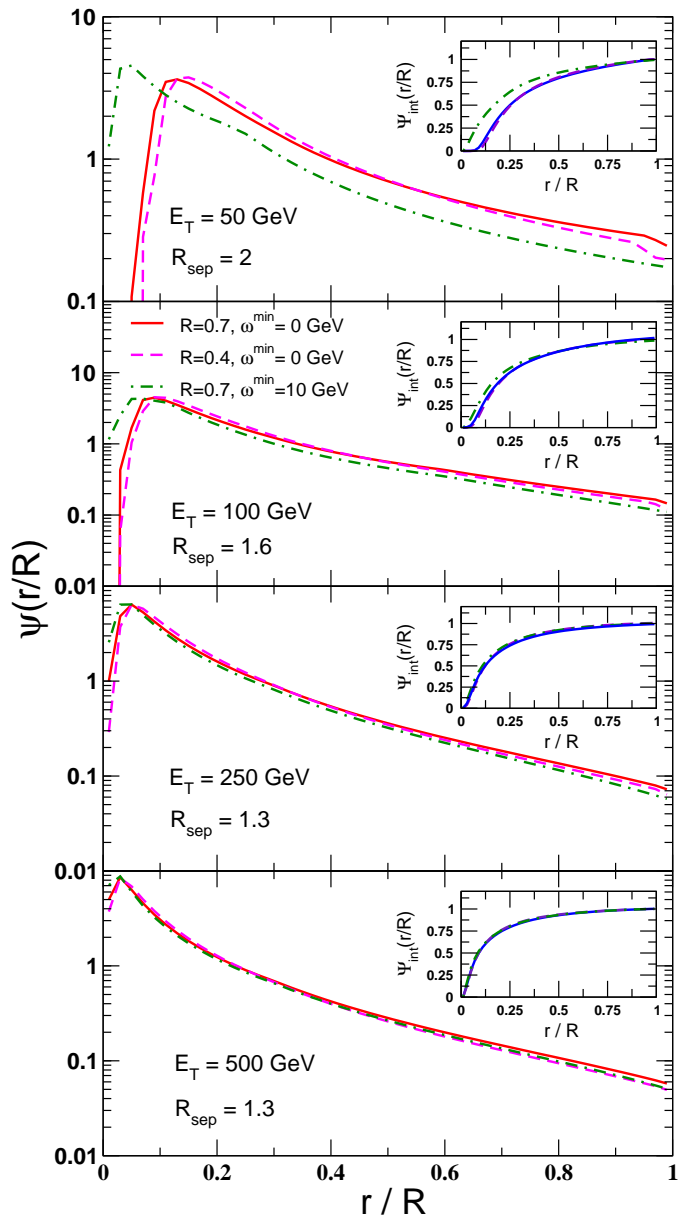


FIG. 2: (Color online) Numerical results for the differential jet shapes in $p+p$ collisions at $\sqrt{s} = 5.5$ TeV at the LHC. Solid lines represent jet shapes with $R = 0.7$, $\omega^{\min} = 0$ GeV, dashed lines stand for jet shapes with $R = 0.4$, $\omega^{\min} = 0$ GeV, and dashed-dotted lines are for jet shapes with $R = 0.7$, $\omega^{\min} = 10$ GeV. The inserts show integrated jet shapes $\Psi_{int}(r; R)$.

particles, must be missed. Thus, even with $p_{T\ min} \sim$ few GeV cuts in $Pb+Pb$ collisions at the LHC aimed at reducing or eliminating the background of bulk QGP particles that accidentally fall within the jet cone, the alteration of $\psi(r/R)$ is expected to be small. We also studied the integral jet shape $\Psi_{int}(r/R)$, shown in the inserts of Fig. 2, as a tool for identifying kinematic and dynamic effects on jets [17]. Only when large differences exist between two $\psi(r/R)$ for $r/R < 0.4$ these will be reflected in the integral jet shape. If the differences are pronounced in

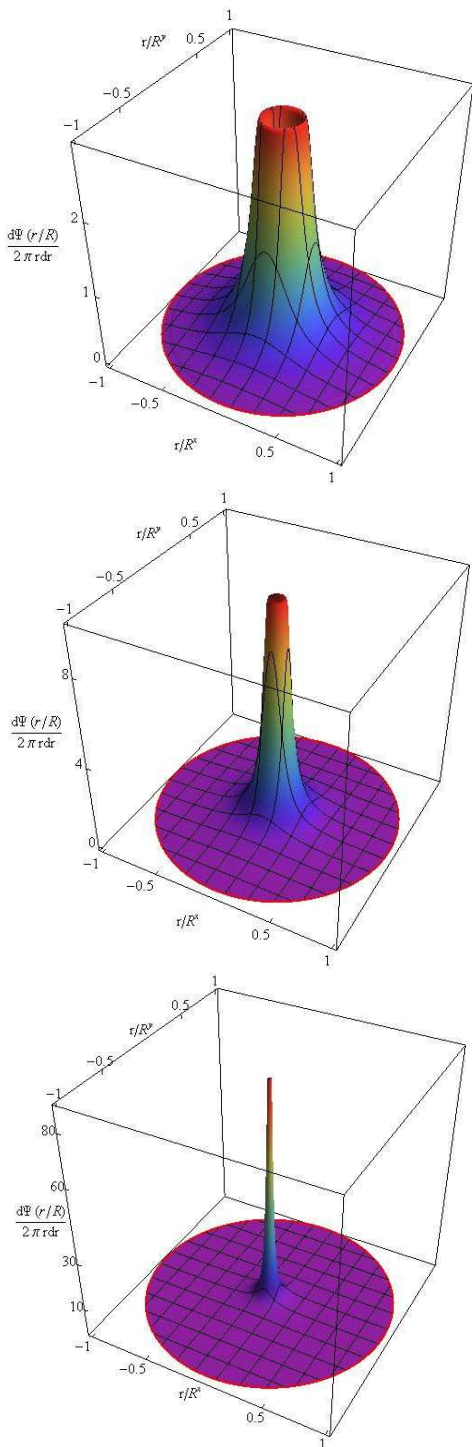


FIG. 3: (Color online) 3D plot of the differential jet shapes at three different jet energies $E_T = 20$ GeV (top panel), $E_T = 100$ GeV (middle panel), and $E_T = 500$ GeV (bottom panel) with $R = 0.7$, $\omega^{\min} = 0$ GeV in $p+p$ collisions with $\sqrt{s} = 5500$ GeV at the LHC. From low jet energy to high jet energy, jet shape becomes much steeper.

the $r/R > 0.4$ region, as is typically the case for heavy ion reactions, $\Psi_{\text{int}}(r/R)$ will be practically insensitive to

the QGP effects on jet propagation.

It is important to also note in Fig. 2 that there is a dramatic change in the differential jet shape in going from small to large transverse energies even in $p+p$ reactions. This is best demonstrated on a 3D-plot, where the volume of the jet cone is normalized to unity. Examples of $\frac{d\psi(r/R)}{2\pi r dr}$ for $E_T = 20, 100, 500$ GeV are given in Fig. 3. We have used $R = 0.7$ and $\omega^{\min} = 0$. It is obvious that development of detailed theoretical models and their validation against experimental data in nucleon-nucleon collisions are necessary before any credible conclusions about the modification of the QCD jets in the QGP medium can be drawn.

III. MEDIUM-INDUCED CONTRIBUTION TO THE JET SHAPE

The principal medium-induced contribution to a jet shape comes from the radiation pattern of the fast quark or gluon, stimulated by their propagation and interaction in the QGP. There is a simple heuristic argument which allows one to understand how interference and coherence effects in QCD amplify the difference between the energy distribution in a vacuum jet and the in-medium jet shape [21]. Any destructive effect on the integral average parton energy loss ΔE^{rad} , such as the Landau-Pomeranchuk-Migdal effect, can be traced at a differential level to the attenuation or full cancellation of the collinear, $k_T \ll \omega$, gluon bremsstrahlung:

$$\begin{aligned} \Delta E_{\text{LPM suppressed}}^{\text{rad}} &\Rightarrow \frac{dI^g}{d\omega}(\omega \sim E)_{\text{LPM suppressed}} \\ &\Rightarrow \frac{dI^g}{d\omega d^2k_T}(k_T \ll \omega)_{\text{LPM suppressed}}, \end{aligned} \quad (26)$$

and we indicate the parts of phase space where the modification of the incoherent $dI^g/d\omega d^2k_T$ is most effective.

Indeed, detailed derivation of the coherent inelastic parton scattering regimes in QCD was given in [6]. In all cases, the origin of the LPM suppression can be traced to the cancellation of the collinear bremsstrahlung. The destructive quantum interference is most prominent for final-state radiation, where the large-angle gluon bremsstrahlung was originally discussed in Ref. [22] to first order in opacity. Even though to carry out realistic simulations to higher orders in opacity with full geometry will require computational power beyond what is currently available, we first present an analytic proof that a cone-like pattern of medium-induced emission persists to all orders in the correlations between multiple scattering centers (elementary emitters) and we focus on the case of immediate interest: light quark and gluon jets and final-state bremsstrahlung. Generalization to massive partons can easily be achieved, see e.g. [23], but it is important to note that the effect of a heavy quark mass versus the jet energy depends on the coherent scattering regime [6].

A. Radiative energy loss in the GLV formalism

In our calculation we will use the GLV formalism of expanding the medium-induced radiation in the correlations between multiple scattering centers [6]. We first recall the definitions of the Hard, Gunion-Bertsch and Cascade propagators in terms of the gluon transverse momentum \mathbf{k} and the transverse momentum transfers from the medium \mathbf{q}_i :

$$\mathbf{H} = \frac{\mathbf{k}}{k^2}, \mathbf{C}_{(i_1 i_2 \dots i_m)} = \frac{(\mathbf{k} - \mathbf{q}_{i_1} - \mathbf{q}_{i_2} - \dots - \mathbf{q}_{i_m})}{(\mathbf{k} - \mathbf{q}_{i_1} - \mathbf{q}_{i_2} - \dots - \mathbf{q}_{i_m})^2},$$

$$\mathbf{B}_i = \mathbf{H} - \mathbf{C}_i, \mathbf{B}_{(i_1 \dots i_m)(j_1 \dots j_n)} = \mathbf{C}_{(i_1 \dots j_m)} - \mathbf{C}_{(j_1 \dots j_n)}, \quad (27)$$

The relevant inverse gluon formation times can be written as:

$$[\tau_{(i_1 i_2 \dots i_m)}^f]^{-1} = \omega_{(i_1 i_2 \dots i_m)} = [k^+ |\mathbf{C}_{(i_1 i_2 \dots i_m)}|^2]^{-1}. \quad (28)$$

For final-state radiation, the intensity spectrum reads:

$$k^+ \frac{dN^g(FS)}{dk^+ d^2\mathbf{k}} = \frac{C_R \alpha_s}{\pi^2} \sum_{n=1}^{\infty} \left[\prod_{i=1}^n \int \frac{d\Delta z_i}{\lambda_g(z_i)} \right] \left[\prod_{j=1}^n \int d^2\mathbf{q}_j \left(\frac{1}{\sigma_{el}(z_j)} \frac{d\sigma_{el}(z_j)}{d^2\mathbf{q}_j} - \delta^2(\mathbf{q}_j) \right) \right]$$

$$\times \left[-2 \mathbf{C}_{(1, \dots, n)} \cdot \sum_{m=1}^n \mathbf{B}_{(m+1, \dots, n)(m, \dots, n)} \left(\cos \left(\sum_{k=2}^m \omega_{(k, \dots, n)} \Delta z_k \right) - \cos \left(\sum_{k=1}^m \omega_{(k, \dots, n)} \Delta z_k \right) \right) \right], \quad (29)$$

where $\sum_2^1 \equiv 0$ and $\mathbf{B}_{(n+1, n)} \equiv \mathbf{B}_n$ are understood. In the case of final-state interactions, $z_0 \approx 0$ is the point of the initial hard scatter and $z_L = L$ is the extent of the medium. The path ordering of the interaction points, $z_L > z_{j+1} > z_j > z_0$, leads to the constraint $\sum_{i=1}^n \Delta z_i \leq z_L$. One implementation of this condition would be $\Delta z_i \in [0, z_L - \sum_{j=1}^{i-1} \Delta z_j]$ and it is implicit in Eq. (29).

There is an obvious limit of the GLV radiative spectrum when $L \gg \lambda_g \gg \tau_f$, where λ_g is the mean free path of the gluon in a hot QGP. Here, the contributions of the $\cos(\dots)$ terms vanish after integration over the unobserved \mathbf{q}_i or Δz_i due to rapid oscillation. It is easy to see in this limit for $n=1$ that,

$$k^+ \frac{dN^g}{dk^+} = \frac{C_R \alpha_s}{\pi^2} \left\langle \frac{L}{\lambda_g} \right\rangle \int d^2\mathbf{k} \int d^2\mathbf{q}_1$$

$$\times \left\langle \frac{1}{\sigma_{el}} \frac{d\sigma_{el}}{d^2\mathbf{q}_1} \right\rangle [\mathbf{C}_1^2 - \mathbf{H}^2 + \mathbf{B}_1^2]. \quad (30)$$

In the very high energy limit $E \rightarrow \infty$, leading to large \mathbf{k} phase space, a change of variables $\mathbf{k} \rightarrow \mathbf{k} - \mathbf{q}_1$ shows that the first two terms in Eq. (30), cancel, leading to an incoherent Bertsch-Gunion gluon emission in a hot QGP medium with $\langle n \rangle = \frac{L}{\lambda_g}$. By direct inspection one can see that the $n \geq 2$ terms do not contribute. In fact, it is easy to verify that for any bremsstrahlung regime, initial-state, final-state and no hard scattering, this limit

holds [6]. More generally, in this limit it can be shown that the reaction operator $\hat{R} \rightarrow 0$. Naturally, for finite jet energies there will be corrections when $k^+ dN^g/dk^+ d^2\mathbf{k}$ is evaluated numerically with actual kinematic bounds [9].

B. Collinear radiation in GLV formalism

While the example given above illustrates that limits can be imposed and taken in the GLV results, such limits are artificial in that the formation time of the gluon at the emission vertex spans $\tau_f \in (0, \infty)$. The Reaction Operator approach [6], i.e. the GLV formalism, is not an approach of averages: it compares differentially τ_f to the separation between the scattering centers. For example, even when $\mathbf{k} \rightarrow 0$ the formation time can be small or large, depending on the momentum transfers for the medium. Let us investigate this case in more detail: we note that $k^+ \approx 2\omega$ and $\mathbf{k} \approx r\omega\hat{n}$, where r is the angle relative to the jet axis. Here, \hat{n} is a unit vector transverse to the jet axis which defines the azimuthal angle ϕ of gluon emission. Using the results of Eq. (29), the 2D (ϕ, r) angular distribution of gluons at n -th order in the correlated scattering expansion reads:

$$\lim_{r \rightarrow 0} \frac{\omega dN^g}{d\omega d\phi dr} \propto \omega \left[\prod_{j=1}^n \int d^2 \mathbf{q}_j \left(\frac{1}{\sigma_{el}(z_j)} \frac{d\sigma_{el}(z_j)}{d^2 \mathbf{q}_j} - \delta^2(\mathbf{q}_j) \right) \right] \frac{\mathbf{q}_1 + \dots + \mathbf{q}_n}{(\mathbf{q}_1 + \dots + \mathbf{q}_n)^2} \cdot \sum_{m=1}^n \omega r \left(\frac{\mathbf{q}_{m+1} + \dots + \mathbf{q}_n}{(\mathbf{q}_{m+1} + \dots + \mathbf{q}_n)^2} \right. \\ \left. - \frac{\mathbf{q}_m + \dots + \mathbf{q}_n}{(\mathbf{q}_m + \dots + \mathbf{q}_n)^2} \right) \times \left(\cos \left(\sum_{k=2}^m \frac{(\mathbf{q}_k + \dots + \mathbf{q}_n)^2}{2\omega} \Delta z_k \right) - \cos \left(\sum_{k=1}^m \frac{(\mathbf{q}_k + \dots + \mathbf{q}_n)^2}{2\omega} \Delta z_k \right) \right). \quad (31)$$

Here, we have already set $r = 0$ where possible. We can use this general notation as long as we clarify certain special cases: for $m = n$ we have $\cos[(\mathbf{q}_{n+1} + \mathbf{q}_n)^2 \Delta z_{n+1}/2\omega] \equiv 1$. For the transverse propagators and m we have $\omega r(\mathbf{q}_{n+1} + \mathbf{q}_n)/(\mathbf{q}_{n+1} + \mathbf{q}_n)^2 \equiv \hat{n}$. It is known that the leading $n = 1$ contribution to final-state medium-induced radiation leads to $\lim_{r \rightarrow 0} \omega dN^g/d\omega d\phi dr = 0$ [22]. Our goal is to show that this result is general and holds to any order in the expansion. Its implications are that there is very little overlap between the techniques used to compute the “vacuum” and medium-induced contributions to the jet shape. A general proof requires demonstration of the absence of unprotected divergences for any set of momentum transfers $\{\mathbf{q}_i\}$, finiteness of the momentum transfer integrals as $\mathbf{q}_i \rightarrow \infty$ and a mechanism that kills the small-angle contribution.

1. We first look at the large \mathbf{q}_i limit. The transverse propagator contribution itself in Eq. (31) behaves as $\sim 1/\mathbf{q}_i^2$. Furthermore, irrespective of the small \mathbf{q}_i behavior of the momentum transfer distribution from the medium, for large momentum transfers the collisional cross section is suppressed by the Rutherford $\sim 1/\mathbf{q}_i^4$ behavior, ensuring the finiteness of the integrals.
2. Next, we examine the potential singularity as $|\mathbf{q}_1 + \dots + \mathbf{q}_n| \rightarrow 0$. The difference in the LPM interference terms in this limit goes as $\mathcal{O}((\mathbf{q}_1 + \dots + \mathbf{q}_n)^2)$ and for the most problematic transverse propagator term ($m=1$) even as $\mathcal{O}((\mathbf{q}_1 + \dots + \mathbf{q}_n)^4)$. In summary, not only is there no divergence in this case, but the integrand in Eq. (31) vanishes.
3. We now collect the interference phases associated with problematic propagators as $|\mathbf{q}_k + \dots + \mathbf{q}_n| \rightarrow 0$, $1 < k \leq n$. Expanding for a small net transverse momentum sums we find that the singularity is canceled:

$$\left[\sin \sum_{j=2}^{k-1} \frac{(\mathbf{q}_j + \dots + \mathbf{q}_n)^2}{2\omega} \Delta z_j \right. \\ \left. - \sin \sum_{j=1}^{k-1} \frac{(\mathbf{q}_j + \dots + \mathbf{q}_n)^2}{2\omega} \Delta z_j \right] \frac{(\mathbf{q}_k + \dots + \mathbf{q}_n)^2}{2\omega} \Delta z_k. \quad (32)$$

Actually, the lack of singularities persists also away from the small r limit.

4. With the integrand well behaved and all integrals finite we see that the phase space factor r in the numerator is sufficient to ensure vanishing medium-induced bremsstrahlung contribution at the center of the jet. It is assisted by partial cancellation from angular integrals of the type $\int \mathbf{q}_i \cdot \mathbf{q}_j f(\mathbf{q}_i, \mathbf{q}_j) d\phi_{ij}$. It is only for the special case of $\hat{n} \cdot (\mathbf{q}_1 + \dots + \mathbf{q}_n)$ where the antisymmetric integrand under $\mathbf{q}_i \rightarrow -\mathbf{q}_i$ for all i fully ensures the vanishing zero-angle radiative contribution.

This completes our proof that at any order in opacity

$$\lim_{r \rightarrow 0} \frac{\omega dN_{\text{med}}^g}{d\omega d\phi dr} = 0. \quad (33)$$

Numerical simulations, using Monte-Carlo techniques, confirm independently that $dI^g/d\omega d^2 \mathbf{k}$ vanishes as $\mathbf{k} \rightarrow 0$ [9].

C. Numerical methods and QGP properties

Results relevant to the LHC phenomenology are calculated using full numerical evaluation of the medium-induced contribution to the observed jet shapes and the modification of the in-medium jet cross sections. Jet production, being rare in that $\sigma(E_T > E_{T \text{ min}}) T_{AA}(b) \ll 1$, follows binary collision scaling $\sim d^2 N_{\text{bin.}}/d^2 \mathbf{x}_\perp$. In contrast, the medium is distributed according to the number of participants density $\sim d^2 N_{\text{part.}}/d^2 \mathbf{x}_\perp$. Soft particles that carry practically all of the energy deposited in the fire ball of a heavy ion collision cannot deviate a lot from such scaling. We take into account longitudinal Bjorken expansion since transverse expansion leads to noticeable corrections only in the extreme $\beta_T \rightarrow 1$ limit [24]. In our approach all relevant finite time and finite kinematics integrals, such as the ones over the separation between the scattering centers $\Delta z_i = z_i - z_{i-1}$, the bremsstrahlung gluon phase space $\Lambda_{QCD} < \omega < E_{\text{jet.}}$, $\Lambda_{QCD} < k_\perp < 2\omega$ [43], and the transverse momentum transfers $0 < q_i < \sqrt{s}/4 = \sqrt{m_D E_{\text{jet}}/2}$, are done numerically [6]. In our simulation we generated in-plane jets, $\phi_{\text{jet}} - \phi_{\text{reaction plane}} = 0$. This is of little importance in central Pb+Pb collisions ($b=3$ fm), where the medium effects on jet propagation are most pronounced, but in semi-central ($b=8$ fm) and peripheral ($b=13$ fm) reactions this will lead to smaller than average energy loss.

The evolving intrinsic momentum and length scales in the QGP expected to be created at the LHC are determined as follows: we first estimate the QGP formation time $\tau_0 = 1/\langle p_T \rangle = 0.23$ fm, where $\langle p_T \rangle \approx 850$ MeV is obtained from extrapolations to LHC energies made by using Monte Carlo event generator results, fit to the CDF collaboration data from $\sqrt{s} = 1.8$ GeV $p + \bar{p}$ collisions [25]. Here we account for the observed $\sim 25\%$ increase in the mean transverse momenta in going from $N + N$ to $A + A$ collisions at RHIC. Gluons dominate the soft parton multiplicities at the LHC and their time- and position-dependent density can be related to charged hadron rapidity density in the Bjorken expansion model [26]:

$$\rho = \frac{1}{\tau} \frac{d^2(dN^g/dy)}{d^2\mathbf{x}_\perp} \approx \frac{1}{\tau} \frac{3}{2} \left| \frac{d\eta}{dy} \right| \frac{d^2(dN^{ch}/d\eta)}{d^2\mathbf{x}_\perp}. \quad (34)$$

Here, $dN^{ch}/d\eta = \kappa N_{\text{part}}/2$ with $\kappa \approx 9$ for $\sqrt{s} = 5.5$ TeV.

Table I summarizes characteristics of Pb+Pb collisions at the LHC and initial QGP properties. An inelastic cross section $\sigma_{in} = 65$ mb has been used in an optical Glauber model where necessary. Assuming local thermal equilibrium one finds:

$$T(\tau, \mathbf{x}_\perp) = \sqrt[3]{\pi^2 \rho(\tau, \mathbf{x}_\perp) / 16\zeta(3)}, \tau > \tau_0. \quad (35)$$

The Debye screening scale is given by $m_D = gT$, recalling that we work in the approximation of a gluon-dominated plasma and $N_f = 0$. The relevant gluon mean free path is easily evaluated: $\lambda_g = 1/\sigma^{gg}\rho$ with $\sigma^{gg} = (9/2)\pi\alpha_s^2/m_D^2$. Note that in Table I the quoted initial mean temperatures, Debye screening scales and gluon mean free paths are obtained as averages with the binary collisions weight $T_{AA}(\mathbf{x}_\perp; b)$. In our evaluation we use $g_s = 2.5$, ($\alpha_s = 0.5$) to describe the scattering of the jet with the medium but the QGP-induced bremsstrahlung is calculated with a running $\alpha_s(k_T)$ for emission vertex, similar to the MLLA approach for the vacuum jet shapes.

Evaluation of the medium-induced energy loss and its contribution to jet shapes is numerically expensive. Exact results have been obtained only for $E_{\text{jet}} = 20, 100$ and 500 GeV. We interpolate for other values of interest.

Class	Central	Mid-central	Peripheral
b [fm]	3	8	13
N_{part}	361	165	18
dN^g/dy	2800	1278	137
$\langle T(\tau_0) \rangle$ [MeV]	751	693	426
$\langle m_D(\tau_0) \rangle$ [GeV]	1.89	1.73	1.07
$\langle \lambda_g(\tau_0) \rangle$ [fm]	0.25	0.27	0.46

TABLE I: Summary of the relevant energy loss parameters and initial QGP properties for central, semi-central and peripheral collisions at $\sqrt{s} = 5.5$ TeV collisions at the LHC.

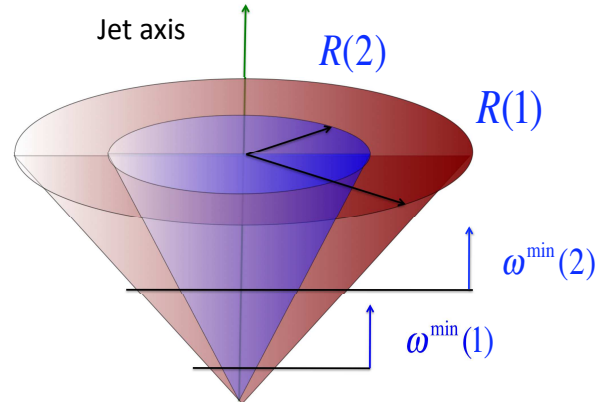


FIG. 4: (Color online) Schematic illustration of the cone radius R and the particle/tower p_T / E_T selection. The measured energy is the one that comes from particles with $p_T > \omega_{\text{min}}$ and within R .

D. Energy loss distribution

A consistent energy loss theory provides complete information for the differential distribution of the lost ΔE_{rad} , i.e. the bremsstrahlung spectrum in Eq. (29). The main point that we make here is that this distribution is completely determined by the properties of the QGP and the mechanisms of energetic quark and gluon stopping in hot and dense matter. Therefore, selecting different jet radii R and $p_{T \text{ min}}$ of the particles will significantly alter both the jet shape and the amount of energy lost by the hard parton which can be recovered in the experimental measurement. In contrast, we have seen in Fig. 2 that the jet shapes scale approximately as a function of r/R , i.e. they are independent of the selection of cone opening angle R . The jet cross section weakly depends on R , unless $R \rightarrow 0$. Finally, $z_{\text{min}} = 0.1 - 0.2$ is necessary to noticeably alter the jet shape, implying that $\sim 20\%$ of the parent parton energy has to be missed via $p_{T \text{ min}}$ cuts to observe significant effects on $\psi_{\text{vac}}(r)$.

Experimentally, a clear strategy will be to use the leverage arms provided by R ($= R^{\text{max}}$ in the evaluation of the ΔE_{rad}) and $p_{T \text{ min}}$ ($= \omega^{\text{min}}$ in the evaluation of the ΔE_{rad}) to determine the distribution of the lost energy. This is illustrated schematically in Fig. 4. Theoretically, the first quantity to be calculated is:

$$\frac{\Delta E^{\text{in}}}{E}(R^{\text{max}}, \omega^{\text{min}}) = \frac{1}{E} \int_{\omega^{\text{min}}}^E d\omega \int_0^{R^{\text{max}}} dr \frac{dI^g}{d\omega dr}(\omega, r). \quad (36)$$

We present in Fig. 5 this fractional energy loss for a quark jet and a gluon jet of energy $E_{\text{jet}} = 20$ GeV inside a jet cone of radius R^{max} and with acceptance cut ω^{min} . Increasing R^{max} or decreasing ω^{min} we will recover more of

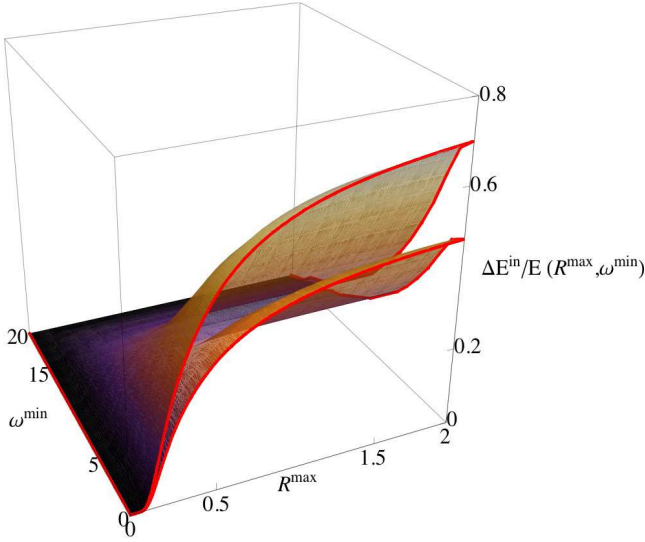


FIG. 5: (Color online) 3D plot for the ratio of the energy that a partons loses inside a jet cone of opening angle R^{\max} with $\omega > \omega^{\min}$ to the total parton energy. We have chosen a jet of energy $E_{jet} = 20$ GeV in $b = 3$ fm Pb+Pb collisions at LHC and varied the jet radius R^{\max} and the acceptance cut ω^{\min} . The upper surface is for a gluon jet and the lower surface is for a quark jet.

the parent parton energy, lost via gluon bremsstrahlung. We note that in Fig. 5 the mean energy loss was calculated as an average over the probability distribution $P(\epsilon; E)$ [27], reflective of multi-gluon fluctuations:

$$\langle \epsilon \rangle = \left\langle \frac{\Delta E}{E} \right\rangle = \int_0^1 d\epsilon \epsilon P(\epsilon; E). \quad (37)$$

For large fractional energy losses, such as in the illustrative example of a 20 GeV jet in central Pb+Pb collisions at the LHC, $\Delta E_g/\Delta E_q$ is much smaller than the asymptotic ratio $C_A/C_F = 9/4$ due to the kinematic constraint $\Delta E < E$ [27].

The separate dependence of $\Delta E^{in}(R^{\max}, \omega^{\min})/E$ on the cone radius and the momentum acceptance cut is more clearly illustrated in Fig. 6. We show central, mid-central and peripheral collisions, impact parameters $b = 3, 8, 13$ fm, respectively, in Pb+Pb reactions at LHC at nominal \sqrt{s} . We notice that, not surprisingly, the ratio $\Delta E^{in}(R^{\max}, \omega^{\min})/E$ goes down at larger impact parameters because the energy loss of the jet decreases in peripheral collisions. More importantly, at each impact parameter there is a variation of the amount of the bremsstrahlung energy, recovered in the cone. This is precisely the variation that will map on the $R_{AA}^{jet}(R^{\max}, \omega^{\min})$ observable. For example, in the limit of a very small opening angle and/or large momentum cut to eliminate the QGP-induced radiation the suppression should approximate that of leading hadrons (up to differences arising from the possibly softer particle spectra

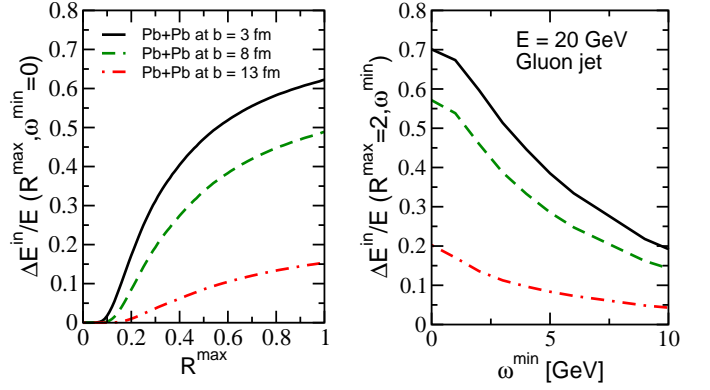


FIG. 6: (Color online) 2D projections of Eq. (36) The left panel shows the fractional energy loss dependence on the jet radius R^{\max} ($\omega^{\min} = 0$) and the right panel shows this dependence versus the acceptance cut ω^{\min} ($R^{\max} = R^{\infty}$). A gluon jet of $E_{jet} = 20$ GeV in $b = 3, 8, 13$ fm Pb+Pb collisions at LHC was used as an example.

due to fragmentation):

$$R_{AA}^{jet}(R^{\max} \rightarrow 0 \text{ and/or } \omega^{\min} \rightarrow E) = R_{AA}^{\text{leading parton}} \approx R_{AA}^{h^{\pm}}. \quad (38)$$

One can see that the typical choices, $R = 0.4$ and $\omega^{\min} = 2$ GeV are a good starting point to explore the variable quenching of jets.

IV. TOMOGRAPHY OF JETS IN HEAVY ION COLLISIONS

The purpose of this Section is to relate the theory of jet propagation in the QGP to experimentally measurable quantities.

A. Experimental observables

An essential ingredient that controls the relative contribution of $\psi_{vac.}(r/R)$ and $\psi_{med.}(r/R) = (1/\Delta E_{rad})dI^g/dr$ to the observed differential jet shape in heavy ion reactions and also determines the attenuation of the jet cross sections is:

$$f \equiv f\left(\frac{R}{R=R^{\infty}}, \frac{\omega^{\min}}{\omega^{\min}=0}\right) = \frac{\Delta E_{rad}\{(0, R); (\omega^{\min}, E)\}}{\Delta E_{rad}\{(0, R^{\infty}); (0, E)\}}, \quad (39)$$

the *fraction* of the lost energy that falls within the jet cone, $r < R$, and carried by gluons of $\omega > \omega^{\min}$ relative to the total parton energy loss without the above kinematic constraints. If this fraction is known together with the probability distribution $P(\epsilon)$ for the parton energy loss

the medium-modified jet cross section per binary $N + N$ scattering can be calculated as follows:

$$\frac{\sigma^{AA}(R, \omega^{\min})}{d^2 E_T dy} = \int_{\epsilon=0}^1 d\epsilon \sum_{q,g} P_{q,g}(\epsilon) \frac{1}{(1 - (1 - f_{q,g}) \cdot \epsilon)^2} \times \frac{\sigma_{q,g}^{NN}(R, \omega^{\min})}{d^2 E'_T dy}, \quad (40)$$

where $E'_T = E_T / (1 - (1 - f_{q,g}) \cdot \epsilon)$. The $(1 - f_{q,g}) \cdot \epsilon$ factor accounts for the total "missed" energy in a jet cone measurement, which necessitates $E'_T > E_T$, and the Jacobian $J = |d^2 E'_T / d^2 E_T|$ is properly accounted for. In this paper possible fluctuations of $f_{q,g}$ independent of ϵ are not considered. Simple analytic limits illustrate the physics represented by Eq. (40): if there is no energy loss, $P(\epsilon) = \delta(\epsilon)$, $J = 1$ and the cross section is unaltered. In the opposite limit, $P(\epsilon) = \delta(\epsilon - 1)$, the quenching of jets, if any, is completely determined by the fraction of the lost energy $f_{q,g}$ that is recovered in the experimental acceptance. When $f_{q,g} = 1$ once again there will be no attenuation of jets and when $f_{q,g} \rightarrow 0$ our result approximates the inclusive particle $R_{AA}(p_T)$ [27], see also Eq. (38).

Next, we obtain the full jet shape, including the contributions from the vacuum and the medium-induced bremsstrahlung:

$$\psi_{\text{tot.}}(r/R) = \frac{1}{\text{Norm}} \int_{\epsilon=0}^1 d\epsilon \sum_{q,g} P_{q,g}(\epsilon) \frac{1}{(1 - (1 - f_{q,g}) \cdot \epsilon)^3} \times \frac{\sigma_{q,g}^{NN}(R, \omega^{\min})}{d^2 E'_T dy} \left[(1 - \epsilon) \psi_{\text{vac.}}^{q,g}(r/R) + f_{q,g} \cdot \epsilon \psi_{\text{med.}}^{q,g}(r/R) \right]. \quad (41)$$

We recall that, by definition, the area under any differential jet shape, $\psi_{\text{tot.}}(r/R)$, $\psi_{\text{vac.}}(r/R)$ and $\psi_{\text{med.}}(r/R)$, is normalized to unity. Integrating over r in Eq. (41), it is easy to see that the correct "Norm" is the quenched cross section, Eq. (40). The interested reader can independently carry out the analysis of the simple limiting cases and gain insight into the dominant contribution to the full jet shape. Proper treatment of isospin is implicit in Eqs. (40) and (41).

B. Energy sum rule

Sum rules provide useful integral representation of conservation laws, originating from symmetries in QCD. One such example is momentum conservation in independent fragmentation:

$$\sum_h \int_0^1 z D_{h/q,g}(z, Q^2) dz = 1, \quad (42)$$

where $z = p_{T,h}/p_{T,q(g)}$ is the momentum fraction of parent partons carried by fragmentation hadrons. The

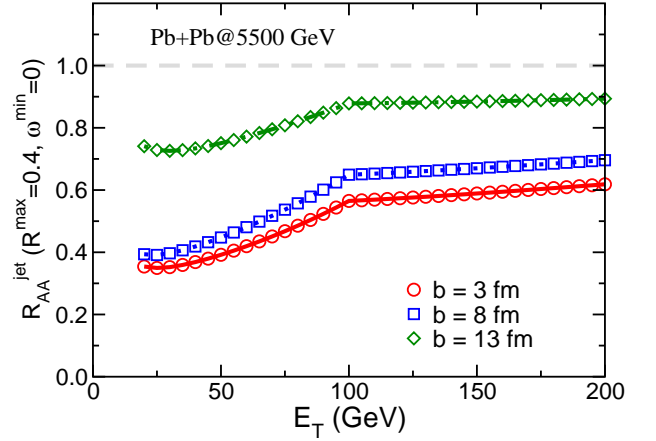


FIG. 7: (Color online) Nuclear modification factor $R_{AA}^{\text{jet}}(R^{\text{max}}, \omega^{\min})$ as a function of the jet transverse energy, E_T , at impact parameters $b = 3$ fm (circle), $b = 8$ fm (square) and $b = 13$ fm (diamond) in Pb+Pb collisions with $\sqrt{s} = 5.5$ TeV.

same sum rule will hold in the presence of a medium since the total momentum of the partons must be conserved irrespective of whether they are propagating in vacuum or in the QGP with/without medium-induced bremsstrahlung [22, 27]. For jets, taking a monochromatic pulse in the vacuum,

$$\frac{1}{\sigma} \frac{\sigma^{NN}}{d^2 E_T} = \delta^2(\mathbf{E}_T - \mathbf{E}_0), \quad (43)$$

we can easily verify that in the presence of a QGP

$$\int d^2 E_T \frac{1}{\sigma} \frac{\sigma^{AA}(R \rightarrow \infty, \omega^{\min} \rightarrow 0)}{d^2 E_T} E_T = E_0, \quad (44)$$

in case of perfect experimental acceptance. More generally, only a fraction, $1 - (1 - f)\langle\epsilon\rangle$, of E_0 is recovered.

C. Numerical results

Combining our full theoretical model for the jet shape and the jet cross section in heavy ion collisions with realistic numerical simulations of parton propagation in the QGP, see Section III C, we first evaluate the nuclear modification factor $R_{AA}^{\text{jet}}(R^{\text{max}}, \omega^{\min})$ in Pb+Pb collisions with center of mass energy $\sqrt{s} = 5.5$ TeV at the LHC. Fig. 7 illustrates the attenuation of the measured jet rate as a function of the jet energy E_T for different centrality classes. We use impact parameters $b = 3, 8, 13$ fm in conjunction with a jet cone radius $R^{\text{max}} = 0.4$ and no acceptance cut ($\omega^{\min} = 0$ GeV). The evolution of $R_{AA}^{\text{jet}}(R^{\text{max}}, \omega^{\min})$ for jets is similar to the one for leading particles in that $\ln R_{AA} \approx -\kappa N_{\text{part.}}^{2/3}$. [27]. However, κ will depend on the selection of R^{max} and ω^{\min} in addition to the steepness of the underlying jet spectra and the properties of the QGP. We recall that the energy

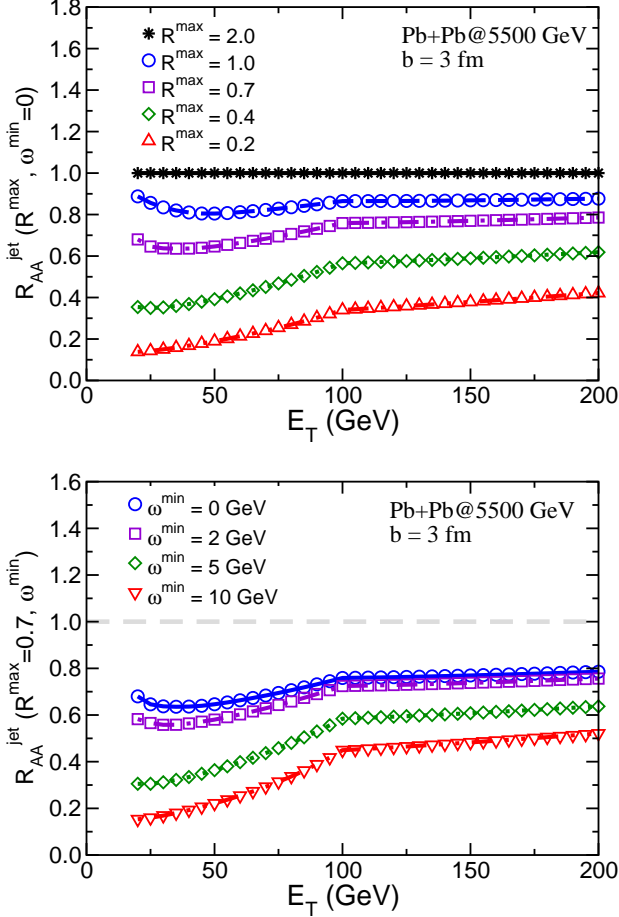


FIG. 8: (Color online) E_T -dependent nuclear modification factor $R_{AA}^{\text{jet}}(R^{\text{max}}, \omega^{\text{min}})$ for different jet cone radii R^{max} (top panel) and at different acceptance cuts ω^{min} (bottom panel) in $b = 3$ fm Pb+Pb collisions at $\sqrt{s} = 5.5$ TeV.

of the jet that will be redistributed out of the cone is $\epsilon(1-f)$, see Eq. (40), and the variation of its quenching with centrality is related to the fractional parton energy loss $\epsilon = \Delta E/E$ and its fluctuations, given by $P(\epsilon)$.

Fig. 8 demonstrates the sensitivity of $R_{AA}^{\text{jet}}(R^{\text{max}}, \omega^{\text{min}})$ to the properties of the medium-induced gluon radiation through the independent variation of ω^{min} and R^{max} , advocated in this paper. For a fixed impact parameter, $b = 3$ fm, the top panel shows a study of the quenching strength versus the jet cone radius when $\omega^{\text{min}} = 0$ GeV. In the approximations that we employ $R^{\text{max}} = 2$ is the upper bound of the medium-induced bremsstrahlung opening angle relative to the jet and, consequently, constitutes perfect experimental acceptance. In this case there is no deviation from binary collisions scaling. The smooth evolution of $R_{AA}^{\text{jet}}(R^{\text{max}}, \omega^{\text{min}})$ with decreasing R^{max} is a signature of the large-angle gluon radiation pattern in the QGP [6, 22]. Note that if $dI^g/d\omega dr$ were predominantly collinear, there would be no deviation from

unity. For $R^{\text{max}} \leq 0.2$ the magnitude of jet quenching approaches the suppression for leading hadrons. A good starting point is a cone radius selection $R^{\text{max}} = 0.4 - 0.7$ if the experimental statistics allows for positive identification of 30% to a factor of 2 variation in the measured cross section. In the bottom panel of Fig. 8 we present the sensitivity of jet attenuation to the minimum particle momentum/calorimeter tower energy deposition cut ω^{min} . For a finite $R^{\text{max}} = 0.7$ even if $\omega^{\text{min}} = 0$ GeV $R_{AA}^{\text{jet}}(R^{\text{max}}, \omega^{\text{min}})$ does not reach unity, see our discussion above. The largest variation in the quenching strength is observed between $\omega^{\text{min}} = 2$ GeV and $\omega^{\text{min}} = 5 - 10$ GeV, and reflects the typical energy of the stimulated gluon emissions. We emphasize that, in the GLV approach [6], partons lose energy through \sim few GeV bremsstrahlung gluons [27]. For $\omega^{\text{min}} > 10$ GeV, $R_{AA}^{\text{jet}}(R^{\text{max}}, \omega^{\text{min}})$ approaches again the characteristic leading particle suppression. In summary, for the same centrality, E_T and \sqrt{s} the continuous variation of quenching values may help differentiate between competing models of parton energy loss [28], thereby eliminating the order of magnitude uncertainty in the extraction of the QGP density.

Detailed investigation of $R_{AA}^{\text{jet}}(R^{\text{max}}, \omega^{\text{min}})$ can also indicate whether “elastic” $2 \rightarrow 2$ processes, such as collisional energy loss [29], or “inelastic” $2 \rightarrow 2 + n$ processes, such as bremsstrahlung [2] and hadron dissociation in the QGP [30], dominate the inclusive particle and particle correlation quenching. If the energy loss *per interaction* in the first scenario $\Delta E_{\text{coll.}}/E \leq 5\%$, the recoil parton from the medium will accelerate almost transversely relative to the jet axis and will not be part of the jet for any reasonable selection of R^{max} . Therefore, for collisional energy loss, in contrast to the well-defined evolution of the jet suppression with cone radius and the acceptance cut seen in Fig. 8, the cross section attenuation will be large and constant and will approximate the quenching of leading hadrons. Note that $R_{AA}^{\text{jet}} < 1$ has also been observed in Monte-Carlo simulations of jet quenching [31].

We now turn to the numerical results for the jet shape in Pb+Pb collisions at $\sqrt{s} = 5.5$ TeV at the LHC. In Fig. 9 we first explore the difference between the vacuum and the medium-induced only (E_T given for the parent parton) $\psi(r/R)$ as a function of the impact parameter, jet energy, and the cone radius. We note that in central heavy ion reactions for lower E_T and, in particular, for $R \geq 0.7$ the two differential shapes can be quite similar. The differences become more pronounced for smaller jet radii where the experimental acceptance will subtend the part of phase space with the most effective cancellation of the collinear medium-induced radiation [22]. It is interesting to observe that in going to more peripheral collisions $\psi_{\text{med.}}(r/R)$ becomes slightly wider. The underlying reason is that the LPM destructive interference between the radiation induced by the large Q^2 scattering and the radiation induced by the subsequent interactions in the QGP determines the angular distribution in the bremsstrahlung spectrum. Thus, a small medium size facilitates the resulting cancellation for glu-

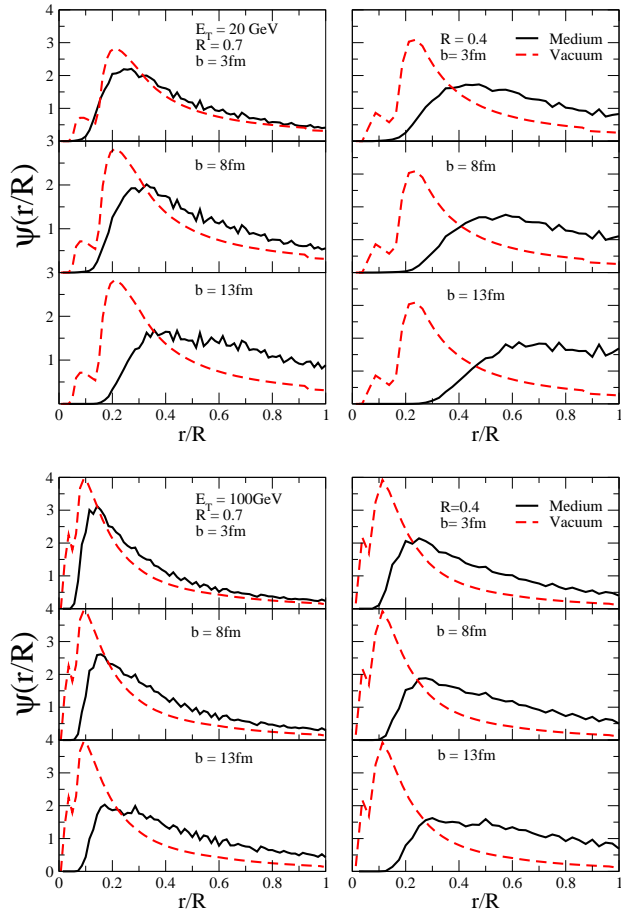


FIG. 9: (Color online) The vacuum and medium-induced only jet shape for $E_T = 20$ GeV (top panel) and $E_T = 100$ GeV (bottom panel) at impact parameters $b = 3, 8, 13$ fm in Pb+Pb collisions at the LHC. Two jet cone radii, $R = 0.7$ and 0.4 are shown.

ons of large formation time. A general observation is that the medium tends to redistribute the flow of energy more evenly inside the jet cone, especially for large $r/R \rightarrow 1$

The pattern of energy flow for in-medium jets is shown in Fig. 10 together with $\psi_{\text{vac.}}(r/R)$ and $\psi_{\text{med.}}(r/R)$ for comparison. We used $E_T = 20$ GeV to 200 GeV and $R = 0.4$ to 0.7 to cover a wide range of measurements that will become accessible during the first year of heavy ion running at the LHC. One observes that there is no significant distinction between the jet shape in the vacuum and the total in-medium $\psi(r/R)$. The underlining reason for this surprising result is that although medium-induced gluon radiation produces a broader $\psi_{\text{med.}}(r/R)$, this effect is offset by the fact that the jets lose a finite amount of their energy, see Figs. 5 and 6. Furthermore, when part of the lost energy is missed due to finite experimental acceptance, the required higher initial virtuality jets are inherently narrower, see Figs. 2 and 3.

In Table II we show the mean relative jet radii $\langle r/R \rangle$ in

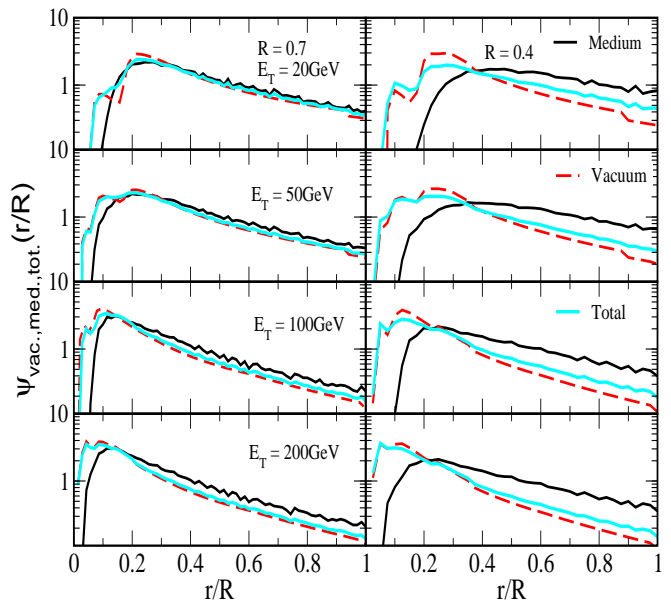


FIG. 10: (Color online) Comparisons of the jet shape in vacuum, the medium-induced jet shape, and the total jet shape for cone radii $R = 0.7$ and $R = 0.4$ and four different energies $E_T = 20, 50, 100, 200$ GeV, respectively, in central Pb+Pb collisions at the LHC.

the vacuum and in the QGP medium created at the LHC for two different cone selections $R = 0.4$ and $R = 0.7$ and four transverse energies $E_T = 20, 50, 100, 200$ GeV. We see that in the realistic numerical simulation there is very little $< 10\%$ increase in the magnitude of this observable. The difference is slightly larger for a smaller cone, since it emphasizes the large-angle character of the medium-induced radiation [6, 22]. Therefore, a rough 1-parameter characterization of energy flow in jets will not resolve the effect of the QGP medium. It can, however, exclude simplistic scenarios of full jet stopping in the QGP that lead to $\langle r/R \rangle$ growth by as much as 60%. It is also important to stress that the QGP is rather “gray” than “black” and only a fraction of the energy of the parent paron is lost via stimulated gluon emission. The effect of even a moderate $\Delta E^{in}(R^{\text{max}}, \omega^{\text{min}})/E$ can be amplified by the steeply falling cross sections for the $R_{AA}^{\text{jet}}(E_T; R^{\text{max}}, \omega^{\text{min}})$ observable, see Fig. 8, but this is not the case for $\langle r/R \rangle$.

Lastly, we point out where the anticipated jet broadening effects will be observed in the differential shape by studying the ratio $\psi_{\text{tot.}}(r/R)/\psi_{\text{vac.}}(r/R)$ in Fig. 11. We have used the same transverse energies and cone radii as in Fig. 10. We recall that the small $r/R < 0.25$ region of the intra-jet energy flow in p+p collisions in our calculation has uncertainties associated with the normalization of the jet shape. In the moderate and large $r/R > 0.25$ region our theoretical model gives excellent descriptions of the Fermilab Run II (CDF II) data, as shown in Fig. 1. The QGP effects are manifest in the “tails” of the energy flow distribution and for a cone radius $R = 0.4$ the ratio could reaches ~ 1.75 when $r/R \rightarrow 1$. However, for

$R = 0.4$	Vacuum	Complete E-loss	Realistic case
$\langle r/R \rangle, E_T = 20\text{GeV}$	0.41	0.55	0.45
$\langle r/R \rangle, E_T = 50\text{GeV}$	0.35	0.48	0.38
$\langle r/R \rangle, E_T = 100\text{GeV}$	0.28	0.44	0.32
$\langle r/R \rangle, E_T = 200\text{GeV}$	0.25	0.40	0.28
$R = 0.7$	Vacuum	Complete E-loss	Realistic case
$\langle r/R \rangle, E_T = 20\text{GeV}$	0.41	0.44	0.42
$\langle r/R \rangle, E_T = 50\text{GeV}$	0.33	0.39	0.37
$\langle r/R \rangle, E_T = 100\text{GeV}$	0.27	0.34	0.29
$\langle r/R \rangle, E_T = 200\text{GeV}$	0.24	0.31	0.26

TABLE II: Summary of mean relative jet radii $\langle r/R \rangle$ in the vacuum, with complete energy loss, and in the QGP medium. Shown are results for cone radii $R = 0.4$ and $R = 0.7$ and transverse energies $E_T = 20, 50, 100, 200$ GeV at $\sqrt{s} = 5.5$ TeV central Pb+Pb collisions at the LHC.

experiments to observe this enhancement of the ratio of

the total jet shape in medium to jet shape in vacuum at $r/R > 0.5$, high statistics measurements will be needed. This precision can hopefully be achieved with the large acceptance experiments at the LHC.

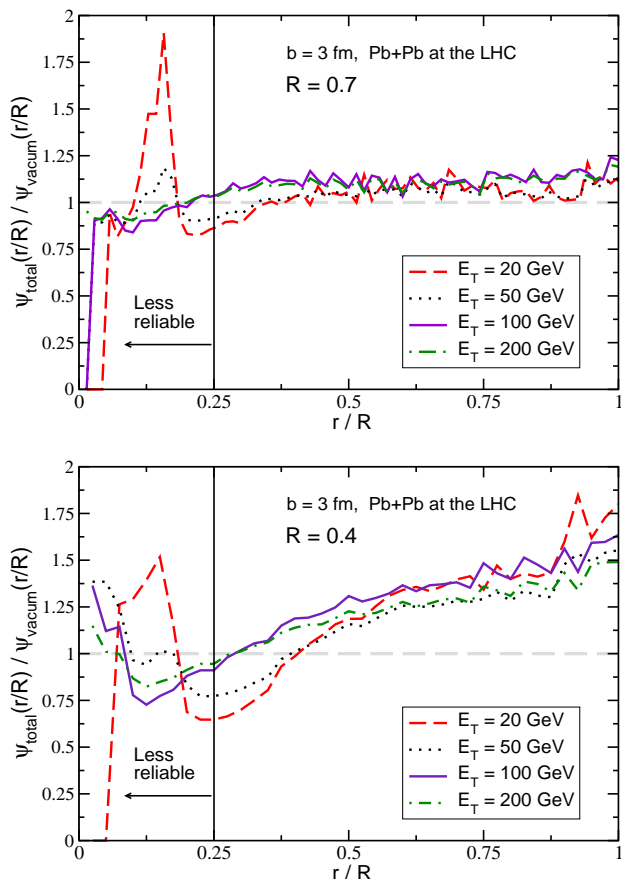


FIG. 11: (Color online) The ratios of total jet shape in heavy-ion collisions to the jet shape in the vacuum for jet energies $E_T = 20, 50, 100, 200$ GeV. Two cone radii $R = 0.7$ (top panel) and $R = 0.4$ (bottom panel) at $b = 3$ fm in Pb+Pb collision with $\sqrt{s} = 5.5$ TeV were chosen.

V. CONCLUSIONS

The unprecedentedly high center of mass energies at the LHC will usher in a new era of precision many-body QCD. The theory and phenomenology of jets in nuclear collisions are expected to evolve as the new frontier in the perturbative studies of parton propagation in the QGP [21]. In this paper we discussed three important aspects of such studies: a generalization of the analytic approach for calculating differential jet shapes [15] that can accommodate experimental acceptance cuts needed to isolate jets in the high multiplicity environment of heavy ion collisions; the theory of the intra-jet energy flow redistribution through large-angle medium-induced gluon bremsstrahlung; and a comprehensive new set of experimental observables that can help identify and characterize the mechanisms of parton interaction in nuclear matter.

In elementary nucleon-nucleon collisions we compared our theoretical model to the CDF II Tevatron data on jet shapes [20] and investigated the baseline $\psi_{\text{vac.}}(r/R)$ at the higher $\sqrt{s} = 5.5$ TeV at the LHC. We found that in the absence of a hot and dense QGP matter these shapes are self-similar and approximately independent of the cone radius R . Elimination of low momentum particles of up to \sim few GeV is not likely to significantly alter the pattern of intra-jet energy flow for $E_T > 50$ GeV jets. In nucleus-nucleus reactions we demonstrated that the characteristic large-angle QGP-stimulated gluon emission [22] persists to all orders in the correlation between the elementary bremsstrahlung sources. We showed that this intensity spectrum can be fully characterized by the amount of the lost energy that falls inside the jet cone ($r < R^{\text{max}}, \omega > \omega^{\text{min}}$) and derived the medium modifica-

tion of the jet shapes and jet cross sections in the QGP, subject to an intuitive energy sum rule.

To demonstrate the connection between the QGP properties, the mechanisms of parton interaction and energy loss in hot and dense matter, and a new class of jet-related experimental observables, we carried out realistic simulations of quark and gluon production and propagation in the medium created in relativistic heavy ion collisions at the LHC. We introduced a natural generalization of the leading particle suppression to jets and showed that it is a more differential and powerful tool that can be used to assess in approximately model-independent way the characteristic properties of the induced gluon intensity spectrum. Consequently, in the future progress can be made toward identifying the set of approximations [2, 5, 6, 7] that most adequately reflect the dynamics of hard probes in the QGP. We also discussed how the evolution of $R_{AA}^{\text{jet}}(R^{\text{max}}, \omega^{\text{min}})$ with the jet cone radius R^{max} and the acceptance cut ω^{min} , or the lack thereof, can help differentiate between radiative and collisional energy loss paradigms of light and heavy quark attenuation. The theoretical approach, developed in this manuscript, allows to investigate the correlation between the quenching of jets and the in-medium modification of their shape. Surprisingly, up to five-fold attenuation of the cross section corresponds to a rather modest $\leq 10\%$ growth of the mean relative cone radius $\langle r/R \rangle$. The anticipated broadening of jets is most readily manifest in the periphery of the cone, $r/R \rightarrow 1$, and for smaller radii, e.g. $R^{\text{max}} = 0.4$.

Further refinements in jet phenomenology, especially the consideration of jet cross sections, should include cold nuclear matter effects, such as nuclear shadowing, the Cronin effect, and initial state energy loss [32]. We finally note that the study of inclusive jet shapes and cross sections in heavy ion collisions can easily be generalized to hadron, photon or di-lepton tagged jets [13, 33, 34] with the benefit of additional constraints on the hard process virtuality and the parton energy.

Acknowledgments

We thank M. H. Seymour, H. Caines, N. Grau and H. Takai for many helpful discussions. This research is supported by the US Department of Energy, Office of Science, under Contract No. DE-AC52-06NA25396 and in part by the LDRD program at LANL, the NNSF of China and the MOE of China under Project No. IRT0624.

APPENDIX A: JET CROSS SECTIONS

In this paper we focus exclusively on large momentum transfer processes, $Q^2 \gg \Lambda_{\text{QCD}}^2$, that can be systematically calculated in the framework of a reliable theory, the perturbative QCD factorization approach. Factorization not only separates the short- and long-distance QCD dy-

namics but implies universality of the parton distribution functions (PDFs) and fragmentation functions (FFs) and infrared safety of the hard scattering cross sections. For hadronic collisions, one of the most inclusive processes is jet production. To lowest order (LO) the invariant differential cross section reads [35]:

$$\frac{d\sigma_{h_a h_b}}{dy_c d^2 p_{Tc}} = K \sum_{abcd} \int_{y_d^{\text{min}}}^{y_d^{\text{max}}} dy_d \frac{\phi_{a/h_a}(x_a, \mu_f) \phi_{b/h_b}(x_b, \mu_f)}{x_a x_b} \times \frac{\alpha_s^2(\mu_r)}{s^2} |\overline{M}_{ab \rightarrow cd}|^2. \quad (\text{A1})$$

Here, $s = (P_a + P_b)^2$ is the squared center of mass energy of the hadronic collision and $x_a = p_a^+ / P_a^+$, $x_b = p_b^- / P_b^-$ are the lightcone momentum fractions of the incoming partons. In this formulation, for massless initial-state quarks and gluons,

$$y_d^{\text{max}(\text{min})} = +(-) \ln \left(\frac{\sqrt{s}}{m_{Td}} - \frac{m_{Tc}}{m_{Td}} e^{+(-)y_c} \right), \quad (\text{A2})$$

where $m_{T_i}^2 = m_i^2 + p_{T_i}^2$. In Eq. (A1) $\phi_{i/h_i}(x_i, \mu_{f_i})$ is the distribution function of parton “ i ” in the hadron h_i and μ_r and μ_{f_i} are the renormalization and factorization and scales, respectively. In this work calculations are done strictly in the collinear factorization approach and we use the CTEQ6.1 LO PDFs [36]. $|\overline{M}_{ab \rightarrow cd}|^2$ are the squared matrix elements for $ab \rightarrow cd$ partonic sub-processes.

Numerical results for inclusive jet cross sections in high energy hadronic collisions are shown in Fig. 12, here $p_T = E_T$. The top panel compares the LO calculation, Eq. (A1), to CDF data on jet cross sections in $p + \bar{p}$ at $\sqrt{s} = 1.96$ TeV. Excellent agreement between data and the theory using $K = 1.5$, independently extracted from the charged hadron $h^+ + h^-$ differential cross section at the Tevatron. It indicates $\sim 50\%$ next-to-leading order correction. Alternatively, we have studied the sensitivity of the cross section to the choice of the factorization and renormalization scales by varying $\mu_r = \mu_f = p_T/2$, p_T and $2p_T$. Not surprisingly, the uncertainty is also on the order of $\sim 50\%$, similar to the phenomenological K -factor. Jet shapes depend on the parton species, quarks versus gluons, and the insert shows the fraction of quark jets versus p_T at the Tevatron. The bottom panel gives predictions for the corresponding jet cross sections at the LHC per nucleon-nucleon collision for $\sqrt{s} = 14$ TeV and 5.5 TeV, without quenching. Insert shows the increased fraction of gluon jets relative to the Tevatron.

We can now evaluate the feasibility of differential jet shape measurements at the LHC. During the first three years of running, even at a fraction of the designed $\mathcal{L} = 10^{34} \text{ cm}^{-2}\text{s}^{-1}$, LHC is expected to deliver an integrated luminosity of 10 fb^{-1} per year. In heavy ion collisions, nominal $\mathcal{L} = 10^{27} \text{ cm}^{-2}\text{s}^{-1}$ is not expected to be achieved either. An integrated luminosity of 1 nb^{-1} per year is a realistic projection. As shown in this paper, the anticipated quenching factor for energetic jets depends on the selection of R^{max} and ω^{min} . In the limit

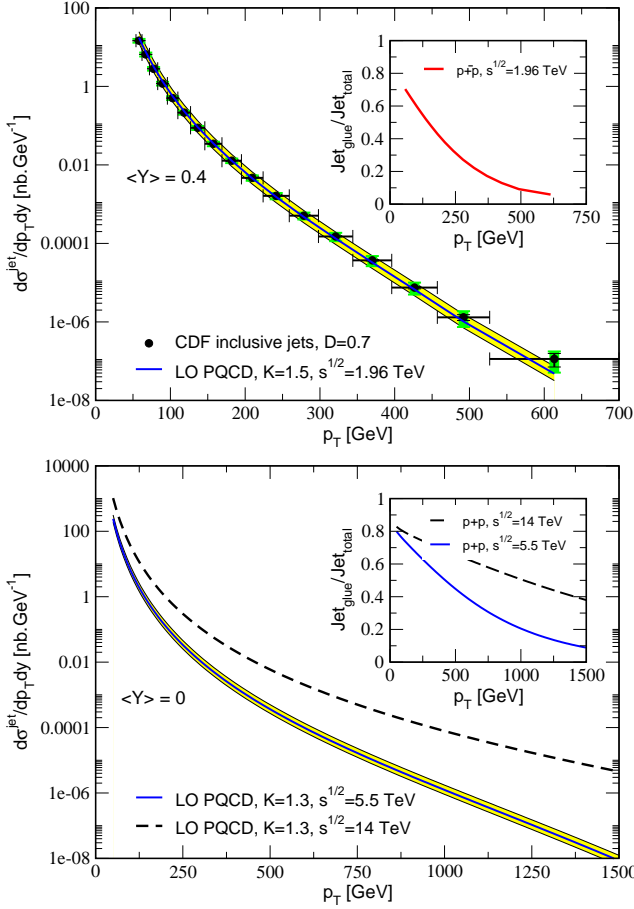


FIG. 12: Top panel: Inclusive jet cross section in $p+\bar{p}$ collisions at the Tevatron $\sqrt{s} = 1.96$ GeV calculated to LO in PQCD and compared to the CDF run II data [37]. Inset shows the fraction of gluon jets as a function of p_T . Bottom panel: predicted baseline jet cross sections in $p+p$ collisions at the LHC at $\sqrt{s} = 5.5$ TeV and 14 TeV.

of narrow jets $R_{AA}^{jet} \approx R_{AA}^{h^\pm} = 0.25 - 0.5$ [27, 29]. Taking this into account, but neglecting for the moment the complications associated with jet reconstruction in the high particle multiplicity environment of heavy ion collisions [14], from Fig. 12 we find that excellent $< 10\%$ statistical precision can be achieved for inclusive measurements of jets of p_T as high as 160 GeV in Pb+Pb reactions and 1.3 TeV in $p+p$ reactions. Jet *shape* measurements require higher statistics since the shape functions are precipitously falling as of $r/R \rightarrow 1$. We expect that very good, $< 30\%$ at large $r/R \sim 1$, *jet shape* measurements will be possible to p_T as high as 100 GeV and 900 GeV in Pb+Pb and $p+p$ collisions, respectively. These will give an indication as to whether medium-induced broadening is present in the tails of the intra-jet energy distribution. The estimates presented in this appendix are conservative, $\Delta y = 1$.

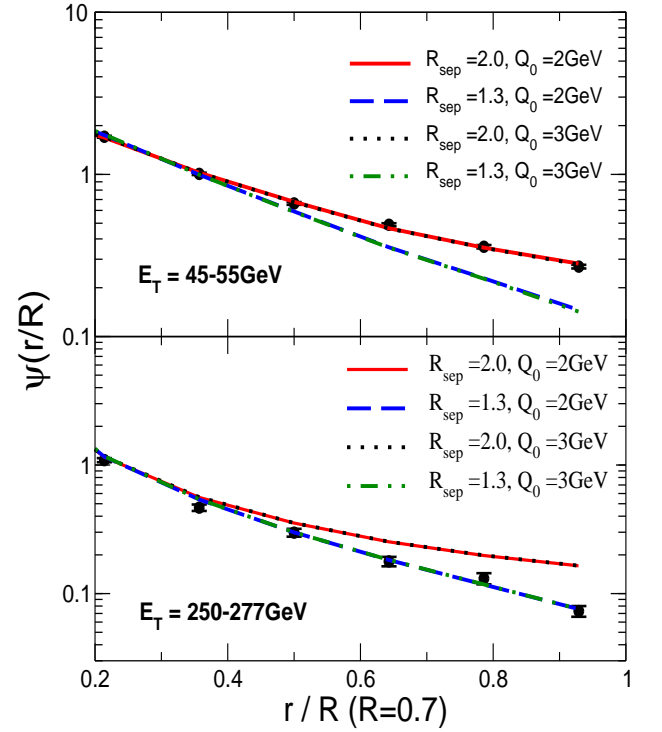


FIG. 13: (Color online) Comparison of the theoretically computed jet shapes with $R_{sep} = 1.3, 2$ and two different non-perturbative correction scales $Q_0 = 2.0$ GeV and 3.0 GeV to experimental data [20]. A jet cone radius $R = 0.7$ was chosen in $\sqrt{s} = 1960$ GeV $p + \bar{p}$ collisions by CDF II.

APPENDIX B: CONTRIBUTIONS TO THE VACUUM JET SHAPE

It is important that a jet finding algorithm be infrared and collinear safe. In full Monte-Carlo simulations of high-energy hadronic events the algorithm can be “tested” and matched to the experimental measurement techniques. In analytic calculations an approximate way to mimic the effect of jet splitting/merger is to introduce an adjustable parameter, R_{sep} , for cone type algorithms. If two partons are within an angle $R_{sep}R$ of each other, they should be merged into one jet [38]. This approach may not be optimal [15] since it does not generalize intuitively for NLO jet shape calculations. When comparing theoretical results to experimental data one finds that R_{sep} is a function of the event kinematics, i.e. it is jet momentum (energy) dependent. Nevertheless, at lowest order this is a useful phenomenological approach to obtain the best possible description of the baseline differential jet shapes in nucleon-nucleon collisions, needed for the study of QGP-induced effects. Also, it is known that for jet cross sections at NLO the results from other jet finding algorithms, such as the fully infrared and collinear safe k_T algorithm with a jet-size parameter D , coincide within a few % with the results from the cone algorithm with appropriate matching/choice of R and R_{sep} [16].

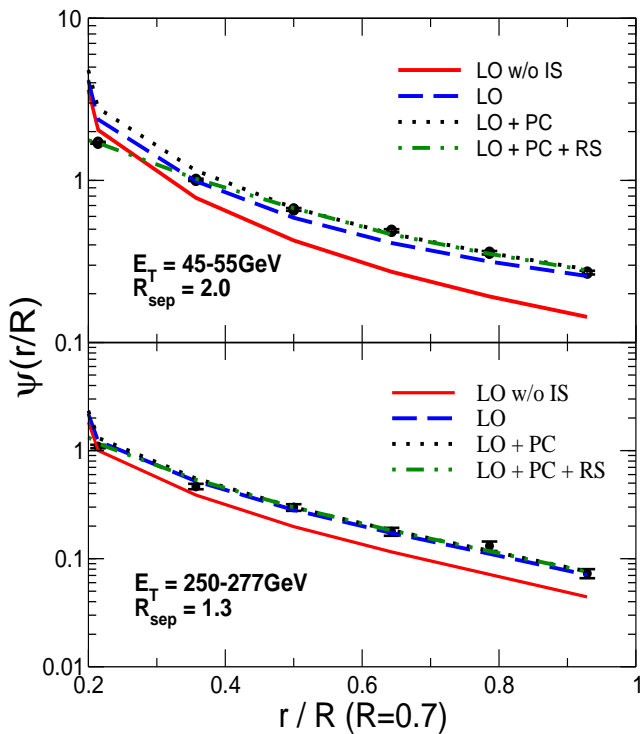


FIG. 14: (Color online) Differential jet shapes in $p + \bar{p}$ collisions at $\sqrt{s} = 1960$ GeV [20] are compared to theory. Leading-order without initial-state radiation (LO w/o IS), leading-order contribution (LO), leading-order with power correction (LO+PC), and leading-order with power correction and Sudakov resummation (LO+PC+RS) results are shown separately.

In Fig. 13 we demonstrate how the numerical results for jet shapes can be optimized using experimental data at the Tevatron. Proper normalization of $\psi(r, R)$ in this Appendix is achieved via first bin subtraction and does not affect the moderate and large r/R part of the energy flow distribution. At low transverse energy, $E_T = 45 - 55$ GeV, a numerical calculation with large $R_{sep} = 2.0$ gives a much better fit than one with a small $R_{sep} = 1.3$. At high $E_T = 250 - 277$ GeV, the theoretical result with small $R_{sep} = 1.3$ agrees with the data by CDF II fairly well. This finding is consistent with a previous study showing that, to fit the data, at low jet E_T one always needs a larger R_{sep} and that R_{sep} should drop with increasing transverse energy [38]. In the numerical calculations shown in Fig. 13 the contribution of power correction to the jet shape has been included. The scale Q_0 is used to separate the non-perturbative effect from the perturbative derivation (see Eqs. (21) and (22)). In Fig. 13 two different values of the non-perturbative correction scale, $Q_0 = 2$ GeV and $Q_0 = 3$ GeV, are used. It is clear that the curves with these two different scales are practically indistinguishable, which demonstrates the consistency of our treatment of non-perturbative effects.

In Fig. 14 we illustrate the influence of the different perturbative and non-perturbative contributions to the

jet shape for different E_T . We observe that the effect of initial-state radiation (IS), absent in lepton colliders, is sizable. In fact, at very high jet energy, a leading-order (LO) calculation with initial-state radiation already gives a good description of the experimental data. However, below ≈ 75 GeV it is impossible to fit the data using only leading order, even with the maximum $R_{sep} = 2$. Other contributions should be considered in an improved theoretical description of jet shapes. These include the effect of the running coupling constant in the momentum transfer integrals (MLLA) and power corrections (PC) $\propto Q_0/E_T$. Sudakov resummation (RS) ensures the finiteness of $\psi(r, R)$ in the region $r \rightarrow 0$. The explicit formulas for these two contributions are given in Section II A. It can be seen from Fig. 14 that all perturbative and non-perturbative effects should be taken into account if reliable description of the experimental results is to be achieved.

APPENDIX C: DOUBLE DIFFERENTIAL MEDIUM-INDUCED JET SHAPE

In this paper we have investigated extensively the differential jet shapes $\psi(r, R) = \frac{d\Psi_{\text{int.}}(r/R)}{dr}$ in vacuum and in heavy-ion collisions at the LHC. This quantity integrates over the energy distribution of the partonic jet fragments. Thus, the information about the angular distribution of soft vs hard shower partons is lost. At the LHC it might be possible, via particle tracking or jet re-analysis, to recover this information on an event-by-event basis and construct $\frac{d^2\Psi(r, R)}{drdz}$, where:

$$\frac{d^2\Psi_{\text{med.}}(r, R)}{drdz} = \frac{1}{\Delta E^{\text{in}}(R, 0)} \frac{dI^g(\omega = zE_{\text{jet}}, r)}{d\omega dr}. \quad (\text{C1})$$

In Eq. (C1) the QGP-induced double differential shape is normalized such that it integrates to unity with $R^{\text{max}} = R$, $\omega^{\text{min}} = 0$ and $z = \omega/E_{\text{jet}}$. To illustrate the additional insight that can be gained through such studies we show numerical results for a simplified case where a quark jet of $E_{\text{jet}} = 100$ GeV propagating through a QGP of length $L = 6$ fm. While the medium is not expanding and characterized by $\lambda_g = 1.5$ fm, $m_D = 0.7$ GeV and $\alpha_s = 0.3$, the $\langle \Delta E/E \rangle$ approximates the full numerical result for central Pb+Pb collisions at the LHC.

Fig. 15 shows a 3D plot of $r \frac{\psi_{\text{med.}}(r, R)}{(2\pi r) dr dz}$ for momentum fraction $z = k^+/E^+ \sim \omega_{\text{gluon}}/E_T = 0.01, 0.03, 0.1, 0.3$ and $R = 1$, $\omega^{\text{min}} = 0$ GeV. We can observe that at $z = 0.01$ ($\omega = 1$ GeV) the double differential medium-induced jet shape is dominated by gluon radiation at large opening angle r/R . At $z = 0.03$ ($\omega = 3$ GeV) the peak lies in the intermediate r/R region with significantly suppressed gluon radiation at small open angle r/R . Increasing ω further narrows the medium-induced intensity profile. It is tempting to associate the characteristic

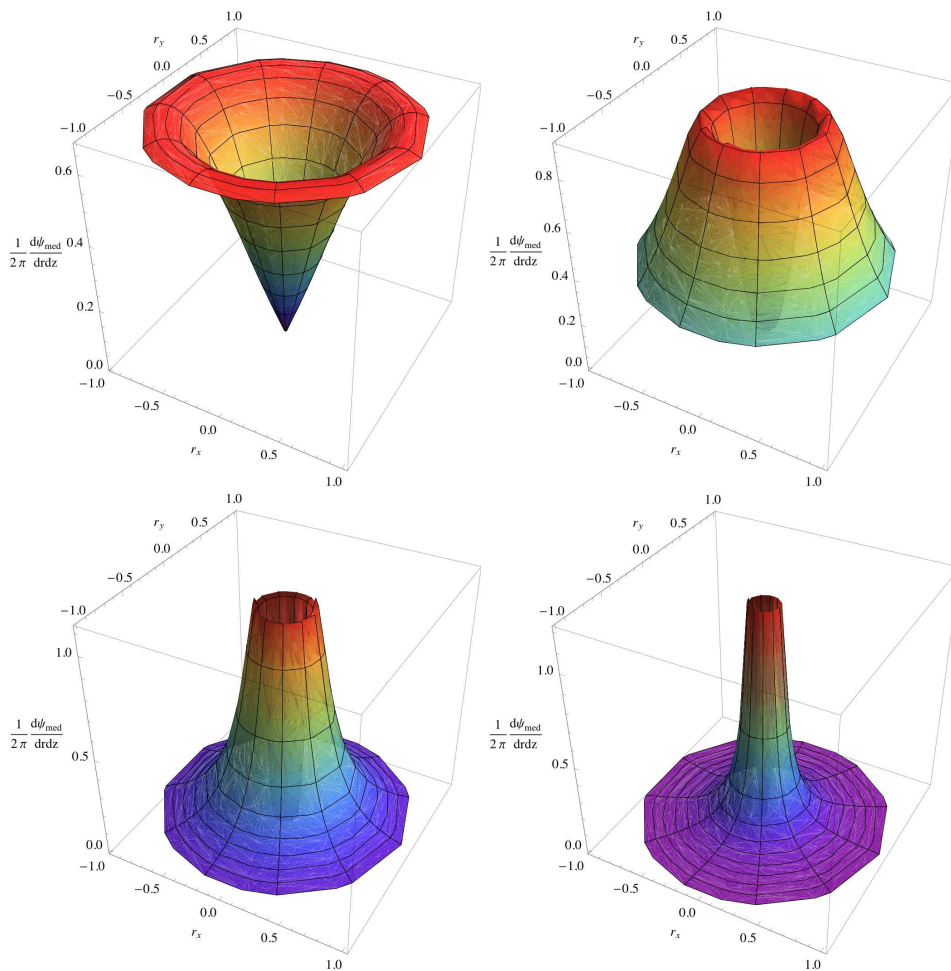


FIG. 15: (Color online) 3D plot of the double differential medium-induced jet shapes for a quark jet of jet energy $E_T = 100$ GeV with $R = 1$, $\omega^{\min} = 0$ GeV in Pb+Pb collisions with $\sqrt{s} = 5500$ GeV at the LHC. Four different figures represent the double differential jet shape for medium-induced gluon momentum fraction $z = 0.01, 0.03, 0.1, 0.3$, respectively.

shapes for small values of z in Fig. 15 with measurements of enhanced away-side large-angle particle-triggered correlations [39, 40, 41]. However, the current RHIC data presents challenges in separating the jet from the background or even distinguishing between events with 1 or 2 minijets (recall that $N_{coll} \sim 1000$ in central Au+Au). Analysis on an event-by-event basis can help reveal un-

ambiguously the QGP medium response to jets. When future experimental measurements of jet in heavy ion collisions are perfected at the LHC full numerical simulations of the double differential shape, including the vacuum and medium-induced components, will soon follow.

-
- [1] X. N. Wang and M. Gyulassy, Phys. Rev. Lett. **68**, 1480 (1992).
 [2] M. Gyulassy, I. Vitev, X. N. Wang and B. W. Zhang, arXiv:nucl-th/0302077.
 [3] A. Adare *et al.* [PHENIX Collaboration], arXiv:0801.4555 [nucl-ex].
 [4] M. M. Aggarwal *et al.* [WA98 Collaboration], Phys. Rev. Lett. **100**, 242301 (2008) [arXiv:0708.2630 [nucl-ex]].
 [5] R. Baier, Y. L. Dokshitzer, A. H. Mueller, S. Peigne and D. Schiff, Nucl. Phys. B **484**, 265 (1997) [arXiv:hep-ph/9608322]; B. G. Zakharov, JETP Lett. **73**, 49 (2001) [Pisma Zh. Eksp. Teor. Fiz. **73**, 55 (2001)] [arXiv:hep-ph/0012360]. N. Armesto, C. A. Salgado and U. A. Wiedemann, Phys. Rev. D **69**, 114003 (2004) [arXiv:hep-ph/0312106].
 [6] M. Gyulassy, P. Levai and I. Vitev, Phys. Rev. Lett. **85**, 5535 (2000) [arXiv:nucl-th/0005032]; I. Vitev, Phys. Rev. C **75**, 064906 (2007) [arXiv:hep-ph/0703002].
 [7] X. N. Wang and X. F. Guo, Nucl. Phys. A **696**, 788 (2001) [arXiv:hep-ph/0102230]; B. W. Zhang and X. N. Wang, Nucl. Phys. A **720**, 429 (2003) [arXiv:hep-ph/0301195].

- [8] P. Arnold, G. D. Moore and L. G. Yaffe, *JHEP* **0206**, 030 (2002) [arXiv:hep-ph/0204343].
- [9] S. Wicks, arXiv:0804.4704 [nucl-th].
- [10] A. Adare *et al.* [PHENIX Collaboration], *Phys. Rev. C* **77**, 064907 (2008) [arXiv:0801.1665 [nucl-ex]].
- [11] S. A. Bass, C. Gale, A. Majumder, C. Nonaka, G. Y. Qin, T. Renk and J. Ruppert, arXiv:0808.0908 [nucl-th].
- [12] J. Collins and J. W. Qiu, *Phys. Rev. D* **75**, 114014 (2007) [arXiv:0705.2141 [hep-ph]].
- [13] D. G. d'Enterria *et al.* [CMS Collaboration], *J. Phys. G* **34**, 2307 (2007). N. Grau [ATLAS Collaboration], *J. Phys. G* **35**, 104040 (2008) [arXiv:0805.4656 [nucl-ex]].
- [14] S. Salur [STAR Collaboration], arXiv:0809.1609 [nucl-ex].
- [15] M. H. Seymour, *Nucl. Phys. B* **513**, 269 (1998) [arXiv:hep-ph/9707338]; M. H. Seymour, arXiv:hep-ph/9707349.
- [16] S. D. Ellis, J. Huston, K. Hatakeyama, P. Loch and M. Tonnesmann, *Prog. Part. Nucl. Phys.* **60**, 484 (2008) [arXiv:0712.2447 [hep-ph]].
- [17] C. A. Salgado and U. A. Wiedemann, *Phys. Rev. Lett.* **93**, 042301 (2004) [arXiv:hep-ph/0310079].
- [18] Y. L. Dokshitzer and B. R. Webber, *Phys. Lett. B* **352**, 451 (1995) [arXiv:hep-ph/9504219].
- [19] C. S. Fischer and R. Alkofer, *Phys. Lett. B* **536**, 177 (2002) [arXiv:hep-ph/0202202].
- [20] D. E. Acosta *et al.* [CDF Collaboration], *Phys. Rev. D* **71**, 112002 (2005) [arXiv:hep-ex/0505013].
- [21] I. Vitev, *J. Phys. G* **35**, 104011 (2008) [arXiv:0806.0003 [hep-ph]].
- [22] I. Vitev, *Phys. Lett. B* **630**, 78 (2005) [arXiv:hep-ph/0501255].
- [23] M. Djordjevic and M. Gyulassy, *Nucl. Phys. A* **733**, 265 (2004) [arXiv:nucl-th/0310076]; B. W. Zhang, E. Wang and X. N. Wang, *Phys. Rev. Lett.* **93**, 072301 (2004) [arXiv:nucl-th/0309040].
- [24] M. Gyulassy, I. Vitev, X. N. Wang and P. Huovinen, *Phys. Lett. B* **526**, 301 (2002) [arXiv:nucl-th/0109063].
- [25] T. Sjostrand, S. Mrenna and P. Skands, *JHEP* **0605**, 026 (2006) [arXiv:hep-ph/0603175].
- [26] C. Markert, R. Bellwied and I. Vitev, arXiv:0807.1509 [nucl-th].
- [27] I. Vitev, *Phys. Lett. B* **639**, 38 (2006) [arXiv:hep-ph/0603010].
- [28] A. Majumder, *J. Phys. G* **34**, S377 (2007) [arXiv:nucl-th/0702066].
- [29] S. Wicks and M. Gyulassy, *J. Phys. G* **34**, S989 (2007) [arXiv:nucl-th/0701088].
- [30] A. Adil and I. Vitev, *Phys. Lett. B* **649**, 139 (2007) [arXiv:hep-ph/0611109].
- [31] I. P. Lokhtin, S. V. Petrushanko, A. M. Snigirev and C. Y. Teplov, *PoS LHC07*, 003 (2007) [arXiv:0706.0665 [hep-ph]]. I. P. Lokhtin, L. V. Malinina, S. V. Petrushanko, A. M. Snigirev, I. Arsene and K. Tywoniuk, arXiv:0809.2708 [hep-ph].
- [32] I. Vitev and B. W. Zhang, arXiv:0804.3805 [hep-ph].
- [33] C. Mironov, P. Constantin and G. J. Kunde, *Eur. Phys. J. C* **49**, 19 (2007).
- [34] N. Grau, B. A. Cole, W. G. Holzmann, M. Spousta and P. Steinberg, arXiv:0810.1219 [nucl-ex].
- [35] I. Vitev, J. T. Goldman, M. B. Johnson and J. W. Qiu, *Phys. Rev. D* **74**, 054010 (2006) [arXiv:hep-ph/0605200].
- [36] J. Pumplin, D. R. Stump, J. Huston, H. L. Lai, P. Nadolsky and W. K. Tung, *JHEP* **0207**, 012 (2002) [arXiv:hep-ph/0201195].
- [37] A. Abulencia *et al.* [CDF II Collaboration], *Phys. Rev. Lett.* **96**, 122001 (2006) [arXiv:hep-ex/0512062].
- [38] M. Klasen and G. Kramer, *Phys. Rev. D* **56**, 2702 (1997) [arXiv:hep-ph/9701247].
- [39] A. Adare *et al.* [PHENIX Collaboration], *Phys. Rev. C* **78**, 014901 (2008) [arXiv:0801.4545 [nucl-ex]]; J. Jia, arXiv:0805.0160 [nucl-ex].
- [40] J. G. Ulery [STAR Collaboration], *Nucl. Phys. A* **783**, 511 (2007) [arXiv:nucl-ex/0609047]; C. A. Pruneau [STAR Collaboration], *J. Phys. G* **34**, S667 (2007).
- [41] L. Molnar, *PoS LHC07*, 027 (2007) [arXiv:0801.2715 [nucl-ex]].
- [42] Some examples include the assumption that the coupling constant $g_s \ll 1$, while $g_s \approx 2$, or the assumption that $L/\lambda_g \rightarrow \infty$ (≥ 10), while $L/\lambda_g \approx 5$. Many jets undergo even fewer interactions in the QGP since they originate in the periphery of the interaction region.
- [43] This condition allows for the deflection of the jet and can be also derived from the finite rapidity range constraint $0 < y_g < y_{\text{jet}}$ for the emitted gluon